Article:
Boudara, V and Read, DJ orcid.org/0000-0003-1194-9273 (2017) Stochastic and pre-averaged non-linear rheology models for entangled telechelic star polymers. Journal of Rheology, 61 (2). 339. ISSN 0148-6055

https://doi.org/10.1122/1.4974908

Stochastic and pre-averaged non-linear rheology models for entangled telechelic star polymers

Victor A. H. Boudara* and Daniel J. Read

School of Mathematics, University of Leeds, LS2 9JT Leeds, U.K.

(Dated: January 11, 2017)

Abstract

We present a simplified stochastic model designed to exemplify the non-linear rheology of entangled supramolecular polymeric materials. We have developed a simplified stochastic model for the rheology of entangled telechelic star polymers. As a toy model for entanglement effects, we use the Rolie-Poly equations [1] that we decorate with finite extensibility. Additionally, we include a stretch-dependent probability of detachment for the stickers. In both linear and non-linear regimes, we explore the parameter space, indicating the parameter values for which qualitative changes in response to the applied flow are predicted. Theory and results in the linear rheology regime are consistent with previous more detailed work of van Ruymbeke and co-workers [2]. Finally, we develop a pre-averaged version of the stochastic equations described above to obtain a set of non-stochastic coupled equations that produces very similar predictions but requires less computing resources. This pre-averaged model is based on two tensors representing the attached and detached chain populations and a scalar quantity that represents the fraction of these populations.

* mmvahb@leeds.ac.uk

I. INTRODUCTION

Telechelic polymers, as introduced by Ref. [3], are defined as polymer molecules possessing functional terminal end-groups. Because these end-groups, also referred to as "stickers", can create transient networks, they modify the (long time) flow properties of the material. By tuning the strength or the nature of the stickers, one can modify the supramolecular structure of the system. Previous theoretical works and simulations have tried to understand the different interactions leading to the self assembling process of non-entangled solutions of linear telechelic polymers [4, 5], or polymers with stickers along the backbone [6–8], or linear entangled polymers with stickers along the backbone [9–11].

Our goal in this paper is to produce a "toy" (i.e. "single mode") constitutive model that captures elements of the non-linear rheology of entangled telechelic polymers, and to explore the interaction between timescales set by the stickers, timescales set by the entangled polymer, and the flow rate. In creating such a toy model, we have chosen to consider a star polymer architecture and, since this does not immediately seem the most obvious choice, we feel it requires some explanation before proceeding. In particular: why we choose a star architecture instead of a linear?

An entangled star arm is pinned at one end by its branch point – which is fixed in our simple model (we ignore, for simplicity, branch point withdrawal [12–15]). Hence, as presented in Figure 1, we consider that the star arm has strictly only two possible states: (i) when the sticker is "attached" then no relaxation is possible – except through convective constraint release in non-linear flows [16] – and the arm is trapped in the entanglement network; (ii) when the sticker is "detached" then relaxation becomes possible by contour length fluctuation (CLF).

In contrast, the other "simple" architecture, telechelic linear chains (with stickers at both ends), have a greater number of states to consider: linear chains can stick together to form longer linear chains, somewhat akin to wormlike micelles [17], which can still relax by reptation (i.e. the stickers do not prevent relaxation, but only increase the reptation time), which, in turn, delays the non-linear effects (stretching of the chains) that we aim at studying here. Moreover, in practice, even stickers designed to be difunctional commonly have additional weaker associations with other stickers, so that they tend to form clusters,

suppressing the reptation [18] – when this occurs the possible relaxation pathways of the material start to become somewhat complex, which wholly defeats the object of our intended "toy" model study.

In some materials, the stickers are actually designed to form clusters rather than pair-wise associations, e.g. zwitterionic groups that forms "clusters of sticker pairs" [2, 19–21]. Telechelic linear chains have stickers at both ends so that release of either sticker could give rise to relaxation of the entangled chain. However, we could assume that, when one sticker is released, the other normally remains attached to its cluster. In this case, the attached cluster acts in a similar way to the branch point in a star polymer, suppressing reptation, so that relaxation is via CLF (breathing modes/arm retraction) [22–24]. Only when both stickers are released can reptation occur (a rare event if the stickers are strong). Again, consideration of these effects gives rise to a greater number of states for the linear chains, as compared to the "simpler" star arm.

Linear chains are therefore more complicated than the star architecture for the purposes of the present study since whether we consider pair-wise association, or clusters of stickers, the star arm is a two-state system whilst the linear chain requires consideration of multiple states. Nevertheless, given the above argument that in practice the relaxation of linear chains shares features with star chains, we might hope that our toy model captures the essence of the non-linear rheology for many linear chain systems. In this sense, we consider our model to be an equivalent of the "pom-pom" model for branched polymers [13, 15] – it is based on a simplified picture of a representative architecture, and designed to capture the essential physics.

Star polymers, first reported in Ref. [25, 26], exhibit unique properties due to their spatially defined and compact three-dimensional compact structure. Efficient synthetic routes and unique rheological properties make them promising tools for use in drug delivery, biomedical applications, or thermoplastics, amongst other applications [27, 28]. Entangled telechelic star polymers have been the focus of previous work where they successfully established a linear rheology model [2]. We now aim at establishing a non-linear rheology model for entangled telechelic stars, that would, in the limit of the linear regime, be compatible with Ref. [2].

We propose a simplified stochastic tube model for telechelic star polymers able to account for both the associating dynamics of telechelic groups and the entanglement constraints. For

simplicity we consider in our model that the stickers are designed to form clusters to avoid the complications arising from bifunctional (pair-wise) associations where partner exchange and the time to search for a new free partner should be considered [7]. In our model, the stickers have a probability to become free (or attached) that does not depend on the surrounding chain states. Nevertheless, we note that more complex sticker dynamics could easily be incorporated into our model.

However simple, our resulting model exhibits interesting constitutive behavior. We find that the nature of the response to flow depends very much on the interaction between timescales set by the entanglements, and timescales set by the stickers. In principle, these timescales vary with temperature (and other factors) in different ways. This leads to (i) thermorheological complexity and (ii) the – perhaps obvious – possibility of using temperature as a control variable to change the processing properties of the material. In order to illustrate these effects, we present "maps" of the parameter space, showing how the response may be expected to change as parameters are varied.

Whilst the stochastic model gives interesting results, it is preferable for flow computations to have a simplified model which exhibits broadly the same behavior. We, therefore, get rid of the stochastic nature of our model by pre-averaging our set of equations. The resulting model, quantitatively very close to that of the stochastic model, is computationally far less expensive and would allow for future flow simulation such as shear banding studies.

In Section II, we develop our stochastic model. The predictions in the linear regime and comparison with previous work are done in Section III. Predictions for non-linear shear and extension are presented in Section IV. Then, the pre-averaged model is presented in Section V and compared against the predictions of the stochastic model. Finally, we summarize the main conclusions in Section VI.

II. STOCHASTIC MODEL

A. Assumptions of the model

We develop a simplified model for entangled star polymers with sticky end groups, as a test model to explore linear and non-linear rheology of entangled supramolecular systems. We explore the effects of interplay between entanglement timescales and sticker lifetimes

within a highly simplified non-linear constitutive model. The entanglement effect gives orientation and stretch relaxation times, $\tau_{\rm d}$ and $\tau_{\rm s}$ respectively, whilst stickers give three (non-independent) parameters: the association lifetime, the free lifetime, and the fraction of associated stickers, $\tau_{\rm as}, \tau_{\rm free},$ and ϕ respectively. Different assumptions about sticker attachment and detachment dynamics have been listed in Ref. [5]. For our initial model development, we have chosen to use the simplest possible assumption for attachment/detachment dynamics [29], but we note that other assumptions could straightforwardly be incorporated into the model. We will match our model parameters with those used in the literature and run simulations to understand how the parameters influence the linear and non-linear rheology. We explore the parameter space and characterize the different system's behavior encountered in each region of it.

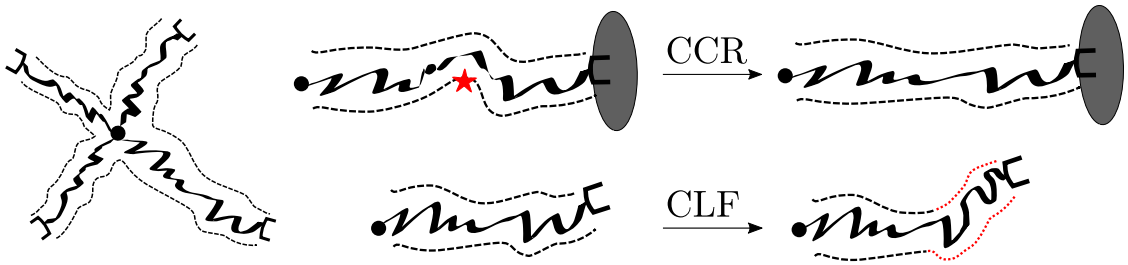

FIG. 1. Left: representation of an entangled telechelic 4-arms star polymer. Each arm has a sticky group " ⊏ " on one end, and is fixed to the branch point " • " on the other end. Right, top: if the sticker is attached (to the grey area), CCR event (red star) contributes to stress relaxation. Bottom: if the sticker is detached, CLF relaxes stress by renewing the tube (red dotted line) – in addition to CCR.

Figure 1 illustrates our model of star polymer. Each arm has a sticky group that can associate and dissociate due to thermal fluctuations. For the purposes of initial model development, we assume that each sticker attaches to, and detaches from, a mean field "sticky background". This is an approximation to the situation where stickers associate to micelles, with many stickers per micelles. On the right is the simplified model we are working with where only two states are possible: either the sticker is attached or detached. Our model is a single arm model. The main ingredients of our model are:

(i) probabilities of association and dissociation of the sticky end group;

(ii) entanglement effects – which give rise to tube orientation and stretching of the chain

within the tube. Although star polymers have a range of relaxation times [22–24], we consider in our model a single orientation relaxation time and single stretch relaxation time; (iii) finite extensibility of polymer chains.

Note that the number of star arms does not appear directly in our model but it would be a crucial parameter for the branch point withdrawal effect, which is not included in our simple model. Branch point withdrawal is, however, unlikely or rare if the number of arms per star is significant. The force balance for branch point withdrawal would require a situation where one arm is significantly stretched whilst all other arms are not stretched. Such situations may occur from time to time, but will not provide the dominant rheological response.

B. Entanglements

As a toy model for entanglements we base our single orientation relaxation time model on the Rolie-Poly equation of Likhtman and Graham [1]. Let us present a brief review of the model and its origins.

Graham and co-workers proposed a molecular theory for entangled polymer chains under fast deformation, referred to as GLaMM model [30]. The GLaMM model includes the processes of reptation, thermal constraint release, chain stretch, and contour length fluctuation (CLF), but differs in the treatment of the convective constraint release (CCR) – as introduced by Marrucci [16] – from previous models [31, 32]. However successful in predicting the rheology of fast flows, the GLaMM model requires solving partial differential equations which means intensive calculations. From the GLaMM model, Likhtman and Graham derived a simplified constitutive equation, called the Rolie-Poly equation (for Rouse linear entangled polymers) [1]. It is a simple one-mode differential constitutive equation for the stress tensor that contains reptation, stretch and CCR. In that theory, the time evolution equation of the conformation tensor of the polymer chain, $\underline{\underline{\boldsymbol{\tau}}}$, is given by

$$\frac{\mathrm{d}\underline{\underline{\boldsymbol{\tau}}}}{\mathrm{d}t} = \underline{\underline{\boldsymbol{\kappa}}} \cdot \underline{\underline{\boldsymbol{\tau}}} + \underline{\underline{\boldsymbol{\tau}}} \cdot \underline{\underline{\boldsymbol{\kappa}}} + \underline{\underline{\boldsymbol{f}}}(\underline{\underline{\boldsymbol{\tau}}}), \tag{1}$$

with the function $\underline{\underline{\boldsymbol{f}}}$ given by

$$\underline{\underline{\boldsymbol{f}}}(\underline{\underline{\boldsymbol{\tau}}}) = -\frac{1}{\tau_\mathrm{d}}(\underline{\underline{\boldsymbol{\tau}}} - \underline{\underline{\boldsymbol{I}}}) - \frac{2}{\tau_\mathrm{s}}\left(1 - \left(3/\operatorname{tr}\underline{\underline{\boldsymbol{\tau}}}\right)^{1/2}\right)\left(\underline{\underline{\boldsymbol{\tau}}} + \beta\left(\operatorname{tr}\underline{\underline{\boldsymbol{\tau}}}/3\right)^{\delta}(\underline{\underline{\boldsymbol{\tau}}} - \underline{\underline{\boldsymbol{I}}})\right), \tag{2}$$

where $\underline{\underline{\boldsymbol{\kappa}}}$ is the velocity gradient tensor, τ_d the reptation or disengagement time, τ_s is the slowest Rouse time or stretch time, β is the CCR parameter as in Ref. [16] and analogous

to c_ν in the GLaMM model, δ is a negative power that can be obtained by fitting to the GLaMM model, and $\underline{\underline{\boldsymbol{I}}}$ is the isotropic or equilibrium tensor.

Our stochastic system is composed of N chains with their own history of attachment/detachment of their sticker. We shall detail our model for the stochastic dynamics of attachment and detachment below, in Section II D. At any given time of the simulation, each chain i has either its sticker attached or detached. If the sticker is detached, we set the stretch relaxation time $\tau_{\mathrm{s},i} = \tau_\mathrm{s}$, and the orientation relaxation time $\tau_{\mathrm{d},i} = \tau_\mathrm{d}$. On the other hand, if the sticker is attached, the chain is anchored between the branch point of the star and the sticker. Therefore, stretch relaxation and orientation relaxation are prohibited, so we set $\tau_{\mathrm{s},i} \to \infty, \tau_{\mathrm{d},i} \to \infty$. Hence as each individual chain in our simulation undergoes its history of detachment and attachment, it switches from being able to relax its stress and stretch, or not. However, surrounding chains are still moving and release entanglement constraints: we allow our N chains to interact with one another via the CCR mechanism. Additionally, we include the finite extensibility of the arm to the Rolie-Poly model using the Warner approximation of the inverse Langevin function [33].

Considering the arm i, the evolution equation of its conformation tensor, $\underline{\underline{\boldsymbol{\tau_i}}}$, reads

$$\frac{\mathrm{d}}{\mathrm{d}t}\underline{\underline{\boldsymbol{\tau_i}}} = \underline{\underline{\boldsymbol{\kappa}}} \cdot \underline{\underline{\boldsymbol{\tau_i}}} + \underline{\underline{\boldsymbol{\tau_i}}} \cdot \underline{\underline{\boldsymbol{\kappa}}}^{\mathrm{T}} - \frac{1}{\tau_{\mathrm{d},i}}(\underline{\underline{\boldsymbol{\tau_i}}} - \underline{\underline{\boldsymbol{I}}}) - \frac{2(1-\lambda_i^{-1})}{\tau_{\mathrm{s},i}}\mathrm{fene}(\lambda_i)\underline{\underline{\boldsymbol{\tau_i}}} + 2\beta\nu\lambda_i^{2\delta}(\underline{\underline{\boldsymbol{\tau_i}}} - \underline{\underline{\boldsymbol{I}}}), \tag{3}$$

where

$$\tau_{\mathrm{d},i} = \begin{cases} \tau_\mathrm{d} & \text{if } i \text{ detached} \\ \infty & \text{if } i \text{ attached} \end{cases} \quad \text{and} \quad \tau_{\mathrm{s},i} = \begin{cases} \tau_\mathrm{s} & \text{if } i \text{ detached} \\ \infty & \text{if } i \text{ attached} \end{cases}$$

$$\lambda_i = (\mathrm{tr}\,\underline{\underline{\boldsymbol{\tau_i}}}/3)^{1/2} \quad \text{is the stretch of the arm,}$$

$$\mathrm{fene}(\lambda_i) = \frac{1-\lambda_{\max}^{-2}}{1-\lambda_i^2\lambda_{\max}^{-2}} \quad \text{is a finite extensibility function,}$$

with $\lambda_{\max}$ the maximal stretch, $\underline{\underline{\boldsymbol{\kappa}}}$ the velocity gradient tensor, and ν the CCR rate defined below in Section II C. For the rest of the study, we take $(\beta, \delta) = (1, -1/2)$, as suggested by Ref. [1]. The stress tensor, $\underline{\underline{\boldsymbol{\sigma}}}$, is obtained by averaging the individual stress contributions from each chain, including the contribution from finite extensibility

$$\underline{\underline{\boldsymbol{\sigma}}} = G\frac{1}{N}\sum_{i=1}^{N}\mathrm{fene}(\lambda_i)\underline{\underline{\boldsymbol{\tau_i}}}, \tag{4}$$

where G is the plateau modulus. In the rest of the document we take $G = 1$ without loss of generality.

C. CCR rate

We consider that the length of the chains in the tube at equilibrium is L_0, the current length of the chain i is L_i, and define the stretch ratio $\lambda_i = L_i/L_0$. The relative velocity between the chain end and the tube when the chain is retracting is $v_{\mathrm{rel},i} = L_0(\lambda_i - 1)/\tau_{\mathrm{s},i}$. At this point, we assume that the number of entanglements per arm is fixed, even when the arm stretches [34–36]. It follows that the average distance between entanglements on an arm increases as the chain stretches. We consider the average distance between entanglements to be $a = a_0\lambda_i$, with a_0 the average distance between entanglements at equilibrium. Therefore, the rate at which the chain end passes the entanglements is

$$\frac{v_{\mathrm{rel},i}}{a} = \frac{L_0(\lambda_i - 1)/\tau_{\mathrm{s},i}}{a_0\lambda_i}. \tag{5}$$

Thus, the average CCR rate, ν, is obtained by summing over the contribution of the N chains, and dividing by the total number of entanglement NL_0/a_0. Including the finite extensibility function, we obtain

$$\nu = \frac{\sum_{i=1}^{N} L_0(\lambda_i - 1)\mathrm{fene}(\lambda_i)/a_0\lambda_i\tau_{\mathrm{s},i}}{NL_0/a_0} = \frac{1}{N}\sum_{i=1}^{N}\frac{1-\lambda_i^{-1}}{\tau_{\mathrm{s},i}}\mathrm{fene}(\lambda_i).$$

We see that only the detached chains contribute to the CCR coefficient because $(\tau_{\mathrm{s},j})_{\mathrm{attached}} \to \infty$. Therefore, we obtain

$$\nu = \frac{1}{N}\frac{1}{\tau_{\mathrm{s}}}\sum_{i,\mathrm{detached}}(1-\lambda_i^{-1})\mathrm{fene}(\lambda_i). \tag{6}$$

D. Sticker dynamics

First, let us consider the association dynamics. In this model, the association dynamics is set to the simplest, yet sensible, expression from a large range of possible assumptions about sticker dynamics [5]. Hence, to model a specific chemical system it is likely that the exact form of the expressions in this section would need to be revisited. This can be done without any significant structural change to the model. Our purpose here is to explore a simple set of assumptions and to illustrate the consequences.

The dynamical equations in the previous section must be integrated numerically, i.e. using a discrete time steps Δt. During any given time step, there is a finite probability that a

free sticker will become attached, or that an attached sticker will become free. Based on the typical time the stickers spend free, τ_{free}, the survival probability that a free sticker becomes associated in a simulation time step Δt is

$$p_{\text{free}\to\text{as}} = 1 - \exp\left(-\frac{\Delta t}{\tau_{\text{free}}}\right).$$

This leads us to the expression for the rate of association, in the limit where $\Delta t \ll \tau_{\text{free}}$

$$r_{\text{free}\to\text{as}} = \frac{p_{\text{free}\to\text{as}}}{\Delta t} \approx \tau_{\text{free}}^{-1}. \tag{7}$$

The higher the value of the parameter τ_{free}, the lower the number of transition from free to attached per unit time.

For the purpose of initial model development, we chose the simplest possible model for the rate of attachment, which is here independent of the flow rate or stretch – in contrast with more detailed models (e.g. Ref. [5] on non-entangled polymers).

The rest of this section aims at defining a *stretch dependent* rate of detachment. Indeed, we expect the rate of detachment to increase as the chain stretches because the energy barrier that the sticker has to overcome to detach is diminished as the arm pulls on the bond. We start by defining the rate of detachment, at equilibrium, and when the arm is not stretched, similarly to the attachment rate:

$$r^{\text{eq}}_{\text{as}\to\text{free}} = \tau_{\text{as}}^{-1}, \tag{8}$$

where τ_{as} is the typical time an attached sticker stays attached. The bigger τ_{as}, the fewer the number of transitions from the attached state to the detached state per unit time. Detailed balance states that, at equilibrium, the total number of chains attaching per unit time equals the total number of chains detaching. This condition gives us a relation between the rate of dissociation for a non stretched arm ($\lambda = 1$) at equilibrium, and the fraction, ϕ, of associated arms at equilibrium:

$$\phi\, r^{\text{eq}}_{\text{as}\to\text{free}} = (1-\phi)\, r_{\text{free}\to\text{as}}, \tag{9}$$

where $r^{\text{eq}}_{\text{as}\to\text{free}} = p^{\text{eq}}_{\text{as}\to\text{free}}/\Delta t$. By substitution of Equations (7) & (8) into Equation (9), we obtain a relation between $\phi, \tau_{\text{as}}, \tau_{\text{free}}$

$$\phi = \frac{\tau_{\text{as}}}{\tau_{\text{free}} + \tau_{\text{as}}}. \tag{10}$$

van Ruymbeke and co-workers suggest that for their experimental systems the average time spent associated is much longer than the average time spent free, i.e. $\tau_{\text{free}} \ll \tau_{\text{as}}$, this leads to a fraction of associated arms at equilibrium close to unity [2]. Typical systems called "sticky" or "supramolecular" are usually designed such that most bonds are formed, so ϕ is close to 1. We note that temperature or chemical modification of the solvent may affect the strength of the stickers, e.g. an increase of temperature deactivates hydrogen bonds; counter-ions inactivates metal-ligands stickers [37]. These might also affect the rate at which supramolecular bonds are formed and broken. Hence a system might be classed as "sticky" (ϕ close to 1) and yet have either a fast or slow rate of bond formation and breaking. Conversely, but perhaps less likely, it could be "not sticky" (small ϕ) but have a slow transition between attachment and detachment. All these parameters are contained in ϕ and τ_{as}.

Under "strong" flows, the arms are stretched. The detachment process depends on the stretch of the arm inside the tube. Indeed, we assume that it is more likely for the sticker to detach when the arm is stretched because the entropic forces are pulling stronger on the sticker.

Following previous work [5, 38], we incorporate the effect of the non-linear spring force on the exit rate (detachment rate) of the sticky group. We write the force acting on the sticker as

$$F(L) = \frac{3k_{\text{B}}T}{N_{\text{K}}b_{\text{K}}^2}\frac{1 - L_{\text{eq}}^2 L_{\text{max}}^{-2}}{1 - L^2 L_{\text{max}}^{-2}}L - f, \tag{11}$$

where $L, L_{\text{eq}}, L_{\text{max}}$ are the current, equilibrium, and maximal length of the arm, respectively; $k_{\text{B}}T$ is the thermal energy, N_{K} is the number of Kuhn segments per arm in equivalent freely jointed chain, and b_{K} is the Kuhn segment length. The first term is the force pulling the arm end (i.e. pulling the sticker) inside the tube, the second term, $f = \frac{3k_{\text{B}}T}{a_0}$, with a_0 the distance between entanglements at equilibrium, is the entropic force pulling the arm-end off the tube (Section 6.4 of Ref. [39]). Note that, because we included the numerator $(1 - L_{\text{eq}}^2 L_{\text{max}}^{-2})$ in the non-linear Warner spring factor, the net force is null at equilibrium, $F(L_{\text{eq}}) = 0$.

The detachment is considered as an activated process. Attached stickers are residing within an energy well, so that they must overcome an energy barrier in order to detach. This energy barrier is reduced by the force $F(L)$ acting over a typical length, r, which is the width of the potential energy well i.e. the "sticky zone". Figure 2 illustrates how pulling

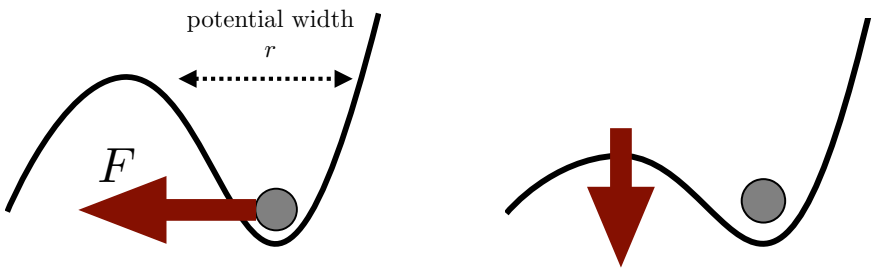

FIG. 2. Schematic representation of the effect of a force, F, pulling on the sticker. The energy barrier that the sticker has to overcome in order to detach is reduced when a force is pulling.

on the sticker reduces the energy barrier that the sticker has to overcome to jump from an attached state to a detached state, i.e. a detachment event is more likely to happen as F grows. Hence, the detachment probability takes the form

$$p_{\text{as}\to\text{free}}(L) \propto \exp\left(\frac{1}{k_{\text{B}}T}\int_{L-r}^{L} F(l)dl\right),$$

with r a length characteristic of the sticker.

After integration we obtain

$$p_{\text{as}\to\text{free}}(L) \propto \exp\left(-\frac{3r}{a_0}\right)\left(\frac{1-L^2L_{\text{max}}^{-2}}{1-L_{\text{max}}^{-2}\left(L-r\right)^2}\right)^{-\frac{3N}{2}\left(1-L_{\text{eq}}^2L_{\text{max}}^{-2}\right)}. \tag{12}$$

When the length of the arm gets close to the maximal value, L_{max}, the probability of detachment diverges and the arm is forced to detach. This result is very similar to Ref. [5] except that (i) in Equation (11), we considered the entropic force f arising from the entanglement effects, (ii) we added the numerator in Equation (11) to have $F(L_{\text{eq}}) = 0$, and (iii) we used a scalar quantity, L, to describe the arm length.

We rewrite Equation (12) using the dimensionless stretch ratio $\lambda = L/L_{\text{eq}} = L/Za_0$, the entanglement number $Z = N_K b_K^2/a_0^2$, and the maximal stretch ratio $\lambda_{\text{max}} = L_{\text{max}}/L_{\text{eq}} = N_K b_K/Za_0$, to obtain

$$p_{\text{as}\to\text{free}}(\lambda) = p_0 \exp\left(-\frac{3r}{a_0}\right)\left(\frac{1-\lambda^2\lambda_{\text{max}}^{-2}}{1-\lambda_{\text{max}}^{-2}\left(\lambda-\frac{r}{Za_0}\right)^2}\right)^{-\frac{3}{2}Z\lambda_{\text{max}}^2\left(1-\lambda_{\text{max}}^{-2}\right)}. \tag{13}$$

We find the proportionality constant, p_0, using Equation (9), and Equation (13) with $\lambda = 1$. It follows the expression for the rate of detachment, $r_{\text{as}\to\text{free}}(\lambda) = p_{\text{as}\to\text{free}}(\lambda)/\Delta t$, of

an associated sticker as a function of the stretch ratio λ:

$$r_{\text{as}\to\text{free}}(\lambda) = \tau_{\text{as}}^{-1}\left(\frac{1-\lambda^2\lambda_{\max}^{-2}}{1-\lambda_{\max}^{-2}\left(\lambda-\frac{r}{Za_0}\right)^2}\,\frac{1-\lambda_{\max}^{-2}\left(1-\frac{r}{Za_0}\right)^2}{1-\lambda_{\max}^{-2}}\right)^{-\frac{3}{2}Z\lambda_{\max}^2\left(1-\lambda_{\max}^{-2}\right)}. \tag{14}$$

Throughout the present work, we assume "typical" values are $Z = 6$, $r/a_0 = 0.01$, $\lambda_{\max} = 10$.

Increasing $\lambda_{\max}$ has a clear impact on the predictions in non-linear shear or extensional flows, at flow rates greater than the inverse effective stretch time or inverse of the association time (timescales defined in Section III), whichever is smaller. In shear flow, at high flow rates, it increases the strain value at which the stress is maximum and also increases the steady state stress value, however, the maximum stress value is nearly unchanged.

In extensional flow, at high extension rates, it increases the maximum and steady state stress value, and the strain at which the maximum stress occurs.

A variation of the ratio r/Za_0 has a small or no impact on the predictions as the ratio has to remain smaller than 1, the reason being that the distance between entanglement at equilibrium, a_0, is bigger than the "sticky length", r, and the entanglement number, Z, cannot be much smaller than 6 for our tube model to hold.

Therefore, some terms of Equation (14) are negligible: $\lambda_{\max}^{-2} \ll 1$, and $\frac{r}{Za_0} \ll 1$. Under these approximations, we obtain a compact form for the rate of detachment

$$r_{\text{as}\to\text{free}}(\lambda) \approx \tau_{\text{as}}^{-1}\left(\frac{1-\lambda^2\lambda_{\max}^{-2}}{1-\lambda_{\max}^{-2}\left(\lambda-\frac{r}{Za_0}\right)^2}\right)^{-\frac{3}{2}Z\lambda_{\max}^2}. \tag{15}$$

E. Numerical implementation

We consider thousands of arms, each arm has its own history of attachment/detachment. When an arm is attached, i.e. the sticker at the arm-end is associated, there is a probability that at the next time step, the sticker will be detached. Similarly, when the arm is free, there is a probability that at the next time step, the sticker will be associated. When the

sticker is associated, we use

$$r_{\text{as}\to\text{free}}(\lambda_i) = \tau_{\text{as}}^{-1}\left(\frac{1-\lambda_i^2\lambda_{\max}^{-2}}{1-\lambda_{\max}^{-2}\left(\lambda_i-\frac{r}{Za_0}\right)^2}\right)^{-\frac{3}{2}Z\lambda_{\max}^2} \tag{16}$$

$$\frac{\mathrm{d}\underline{\underline{\boldsymbol{\tau_i}}}}{\mathrm{d}t} = \underline{\underline{\boldsymbol{\kappa}}}\cdot\underline{\underline{\boldsymbol{\tau_i}}} + \underline{\underline{\boldsymbol{\tau_i}}}\cdot\underline{\underline{\boldsymbol{\kappa}}}^{\mathrm{T}} - 2\beta\nu\lambda_i^{-1}(\underline{\underline{\boldsymbol{\tau_i}}} - \underline{\underline{\boldsymbol{I}}}). \tag{17}$$

When the sticker is detached, we use:

$$r_{\text{free}\to\text{as}} = \tau_{\text{free}}^{-1} \tag{18}$$

$$\begin{aligned}\frac{\mathrm{d}\underline{\underline{\boldsymbol{\tau_i}}}}{\mathrm{d}t} = {}& \underline{\underline{\boldsymbol{\kappa}}}\cdot\underline{\underline{\boldsymbol{\tau_i}}} + \underline{\underline{\boldsymbol{\tau_i}}}\cdot\underline{\underline{\boldsymbol{\kappa}}}^{\mathrm{T}} - 2\beta\nu\lambda_i^{-1}(\underline{\underline{\boldsymbol{\tau_i}}} - \underline{\underline{\boldsymbol{I}}}) \\ & -\frac{1}{\tau_{\mathrm{d}}}(\underline{\underline{\boldsymbol{\tau_i}}} - \underline{\underline{\boldsymbol{I}}}) - \frac{2(1-\lambda_i^{-1})}{\tau_{\mathrm{s}}}\mathrm{fene}(\lambda_i)\underline{\underline{\boldsymbol{\tau_i}}},\end{aligned} \tag{19}$$

Where ν is the CCR rate defined Equation (6), and $\lambda_i = (\mathrm{tr}\,\underline{\underline{\boldsymbol{\tau_i}}}/3)^{1/2}$. Equations (16) and (18) are the rates of detachment and attachment of the stickers. Equations (17) and (19) are the evolution equations that the conformation tensor, $\underline{\underline{\boldsymbol{\tau_i}}}$, follows when the sticker is associated or free, respectively. The total stress is then computed according to Equation (4).

At each simulation time step, Δt, a uniformly distributed random number, $0 < \theta < 1$, is generated, and we compare it with the probabilities of attachment or detachment.
If the sticker is attached and $\theta < r_{\text{as}\to\text{free}}(\lambda_i)/\Delta t$, then the sticker detaches.
If the sticker is detached and $\theta < r_{\text{free}\to\text{as}}/\Delta t$, then the sticker attaches.
Otherwise, the sticker stays in its previous state.
We integrate the above differential equations using Euler's scheme, where we set the time step, Δt, of the simulation to be at least 100 times smaller than the minimum amongst: (i) the sticker timescales, $\tau_{\text{as}}, \tau_{\text{free}}$ (to not miss attachment or detachment events), or (ii) the orientation or stretch relaxation timescales, $\tau_{\mathrm{d}}, \tau_{\mathrm{s}}$, or (iii) the inverse flow rate.

III. PREDICTIONS OF THE MODEL: LINEAR REGIME

A. Method

In order to explore the rheological response of the linear regime of our set of equations presented in Section II, we perform a step strain of 1% in shear, i.e. we apply a strain rate $\dot{\gamma}$ during a short period of time, T, such that $\dot{\gamma}T = 0.01$. Then we monitor the decay of

the dynamic modulus, $G(t)$, while no flow is imposed. In many cases, the decay of $G(t)$ is rather slow, when $\phi \approx 1$, as the stickers remain attached during a time orders of magnitude greater than the simulation time step. Therefore, no relaxation of the modulus G occurs for a long period of time when $\phi \approx 1$.

Indeed, in practice, if $\tau_{\text{free}} \approx 10^{-4}\tau_{\text{as}}$, ($\phi \approx 0.9999$), then $\Delta t = \tau_{\text{free}}/100$ would be the biggest possible time step with Euler's method. It means that to see the first detachment event, likely to happen after a time τ_{as}, one should use 10^6 time steps. Given we consider of order 10^3 chains, we expect 10^9 Euler steps to get to the first detachment event. This number may seem acceptable, but, because multiple detachments are required to fully relax the arms, the simulation time becomes enormous.

We present the method we used to avoid unnecessary long simulations. If the chain is associated, the probability that an associated sticker has not detached during a time Δt is

$$p_{\text{as}\to\text{as}}(\Delta t) = \exp\left(-\Delta t/\tau_{\text{as}}\right).$$

We invert the probability distribution in order to obtain, from a uniformly distributed (pseudo) random number $0 < \theta < 1$, a random time, $(\Delta t)_{\text{detachment}}$, during which the sticker stays attached (or time before detachment). This time is defined as

$$(\Delta t)_{\text{detachment}} = \tau_{\text{as}} \ln(1/\theta).$$

Therefore, we can generate time intervals corresponding to times the sticker spends associated. Similarly, the time intervals corresponding to the time the sticker stays free (or time before attachment) are generated using

$$(\Delta t)_{\text{attachment}} = \tau_{\text{free}} \ln(1/\theta).$$

During the times $(\Delta t)_{\text{detachment}}$ where the sticker is attached, the modulus G for an individual chain stays constant, and relaxation occurs only when the sticker is free. The decay of $G(t)$ for an individual chain during the times, $(\Delta t)_{\text{attachment}}$, when the sticker is free is written as

$$G(t + \Delta t) = G(t) \exp\left(-\Delta t/\tau_{\text{d}}\right). \tag{20}$$

This method allows us to obtain the full relaxation of $G(t)$ in a shorter simulation time than with the classic Euler method. For each chain, we simply generate randomly the history of attachment and detachment in terms of the times between these events, using

the above equations. For each period of time when the chain is detached, we relax the stress according to Equation (20). So, for an individual chain, the stress relaxation becomes a series of plateaus (during the attached state) together with periods of stress relaxation (during the detached state). When averaged over many chains, a smooth relaxation profile $G(t)$ is attained.

From $G(t)$, we use a Schwarzl transformation [40] to reconstruct the elastic and loss moduli G' and G''. In this section the strain applied is small, as a consequence, the system stays in the linear regime and the arms do not stretch ($\lambda = 1$). The stretch relaxation time, τ_s, is, therefore, irrelevant here.

B. Predictions

We are left with three parameters to explore: the orientation relaxation time, the average time a sticky group stays free, and the average time a sticky group stays attached; τ_d, τ_{free}, and τ_{as} respectively. We have found it useful to "map" out our results on a graph with the typical "free" time (τ_{free}) on the horizontal axis, and typical "associated" time (τ_{as}) on the vertical axis. Note that, on a log-log scale, lines of constant fraction of associated chains, ϕ, are parallel lines at 45 degrees to the horizontal and vertical axes. Values of ϕ close to 1 (i.e. sticky systems) are found towards the upper left of the diagram, whilst values of ϕ close to zero (i.e. non-sticky systems) are found towards the bottom right of the diagram. For linear rheology, the values of τ_{free} and τ_{as} should be compared to the orientation relaxation time, τ_d, (whilst in our equivalent maps for the non-linear rheology, Section IV, we compare them against the stretch relaxation time τ_s).

Figure 3 reports the characteristic trends of the loss modulus, $G''(\omega)$, for different values of the parameters. Depending on how τ_{as} and τ_{free} compare with τ_d, different relaxation profiles are seen.

The dashed lines in Figure 3 separate the parameter map into three regions where the loss modulus as a function of the frequency has a clearly different trend.

Between the regions B and C sits the horizontal line that is defined by $\tau_{as} = \tau_d$. Above that line, in the region C, the loss modulus presents two relaxation modes, at frequencies τ_d^{-1} and τ_{as}^{-1}. It is explained as follows: initially, a fraction $(1-\phi)$ of polymer arms is detached, and,

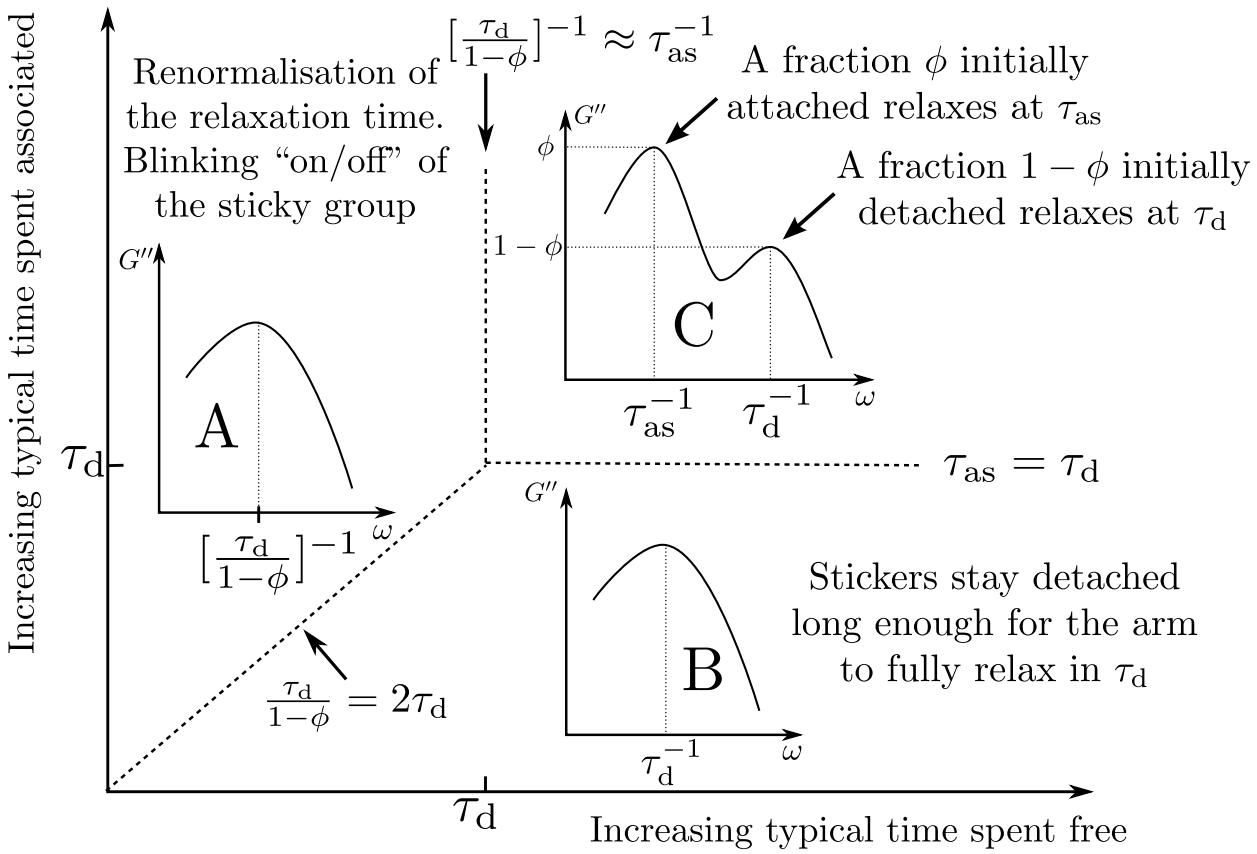

FIG. 3. Sketches of the predictions of our model for frequency sweep, the sub-plots represent the loss modulus as a function of the frequency in log-log scale. Three distinct relaxation behaviors are observed in the region A, B, and C. The discontinuous lines indicate where we expect to see a change in the qualitative shape of G''.

because $\tau_d \ll \tau_{free}$, the stickers stay free long enough so that fraction $(1-\phi)$ of arms can fully relax before the sticky groups reattach. On the other hand, the fraction ϕ of polymers that was initially attached stays attached, in average, during a time τ_{as}. Once they have detached, they can fully relax in a relatively short time τ_d. Thus, the second relaxation mode is located at $\omega = (\tau_{as} + \tau_d)^{-1} \approx \tau_{as}^{-1}$, because $\tau_{as} \gg \tau_d$ in region C.

Below that horizontal line, in the region B, $\tau_{as} \ll \tau_d$, and $\tau_{as} \ll \tau_{free}$. The latter relation means that the sticky groups are mostly detached ($\phi \ll 1$), and the arms can relax their orientation in a time τ_d before the sticky group can possibly attach because $\tau_d \ll \tau_{free}$ in that region. Therefore, we expect the peak in loss modulus to be located at $\omega = \tau_d^{-1}$ similarly to systems with no sticky groups – in fact, in this regime the effect of sticky groups is negligible.

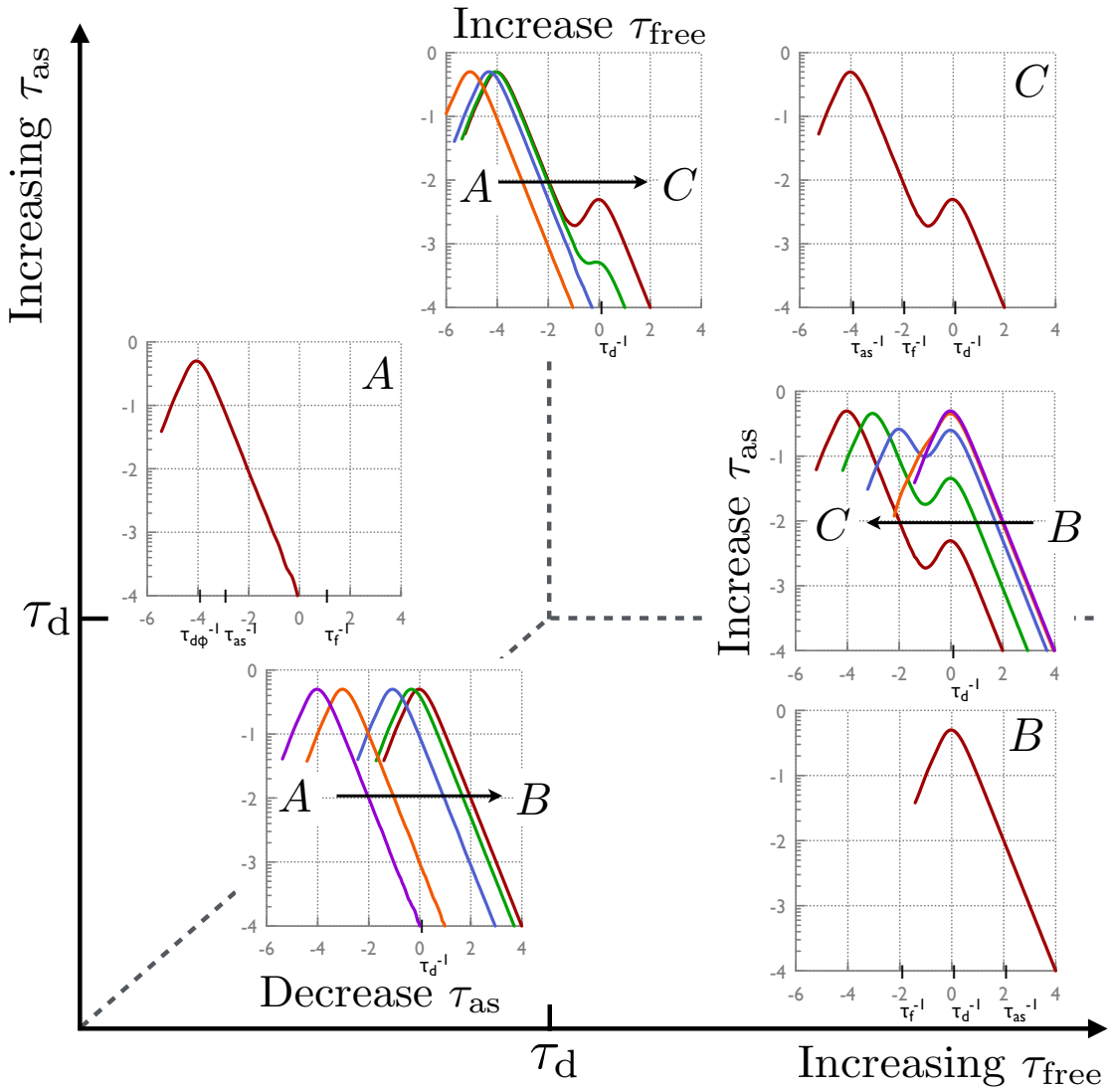

FIG. 4. Predictions in the linear regime. Characteristic behavior of the loss modulus as a function of frequency for each region of Figure 3, and details on what happens when we cross the lines separating the regions A, B, and C.

The vertical line is defined by $\tau_{\text{d}}/(1-\phi) \approx \tau_{\text{as}}$, which occurs, according to Equation (10) and given that $\phi \approx 1$, when $\tau_{\text{free}} = \tau_{\text{d}}$. It separates the region C from the region A. In region A, $\tau_{\text{free}} \ll \tau_{\text{d}}$ and $\tau_{\text{d}} \ll \tau_{\text{as}}$ and the loss modulus relaxation peak is located at $\omega = [\tau_{\text{d}}/(1-\phi)]^{-1}$. The factor $(1-\phi)$ comes from the fact that the sticky group is blinking between the attached and detached states, at a rate which is much faster than the tube orientation relaxation time. The chain is only able to relax stress while detached, which is, on average, a fraction $(1-\phi)$ of the time. Hence the effective relaxation time is increased by the factor $(1-\phi)$ –

this can be considered as an increased "drag" due to the stickers, although the physics of attachment and detachment ensures that the increase in friction is proportional to the bare chain friction.

In other words, during the time after an arm detaches and before it is re-attached, it has time to relax only a small amount of orientation. It then needs to wait for an other detachment event before it can relax more orientation.

The diagonal line separates the region A from the region B. It is defined by $\tau_{\text{free}} = \tau_{\text{as}}$, which, according to Equation (10), is equivalent to $\phi = 1/2$. Thus, on that line we have $\tau_{\text{d}}/(1-\phi) = 2\tau_{\text{d}}$.

Typical simulation results are presented Figure 4, for each of the three regions. We also illustrate the transitions between the regions to show how the loss modulus is affected. From region A to region B, the relaxation peak is moved to lower frequencies as we decrease τ_{as} at constant τ_{free}, i.e. $(1-\phi)$ is increasing. From the region A to the region C, the second relaxation time becomes evident as we increase τ_{free} at constant τ_{as}. Finally, from region B to region C, the second relaxation peak emerges as we increase τ_{as} at fixed τ_{free}.

C. Comparison with literature

We compare our results with experimental data of van Ruymbeke and co-workers [2], where they performed linear rheology measurements on entangled telechelic star polymers. We focus on the 12-arms star polyisoprene functionalized with zwitterionic groups. Figure 5 presents the data for 12PZw-PI-10. Ref. [2] have evidence that some of the arms were not "sticky". One cause could be the synthesis process i.e. some arms do not carry a zwitterionic group (sticker). We expect the fraction of unfunctionalized arms to relax at τ_{d}^{-1}. We observe a bump at intermediate frequencies that we identify with the relaxation of the unfunctionalized arms. At this point, we want to emphasize that our simplified model contains only one orientation relaxation mode, whereas it is known that stars have a broad spectrum of orientation relaxation times [22–24]. Thus, graphically, we can extract a range of values for the orientation relaxation time corresponding to our model: $10^2 < \tau_{\text{d}} < 10^4$ seconds.

On the other hand, for the population of stars with functionalized arms, the sticky groups

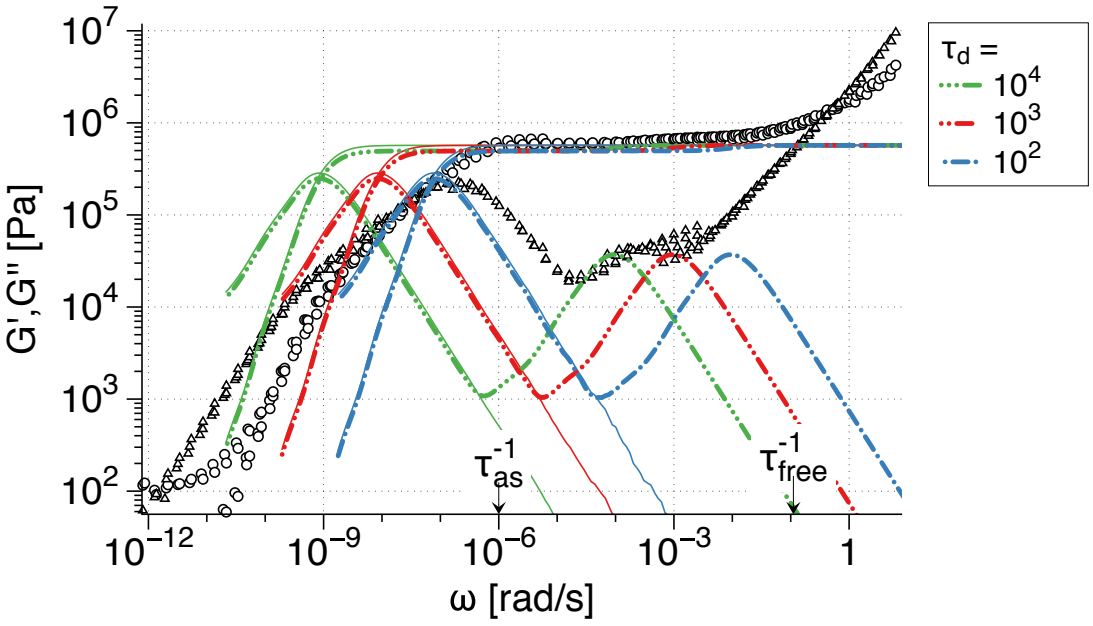

FIG. 5. Linear rheology of 12PZw-PI-10 from Ref. [2] (symbols) together with the predictions of our model for different values of the orientation relaxation time in the range $10^2 < \tau_d < 10^4$ s (thin colored lines). We also present the predictions of our model with 13% of non-functionalized arms (dot-dashed thick lines). [parameters: $\tau_{as} = 10^6$ s, $\tau_{free} = 9$ s, plateau modulus $G_N^0 = 0.57$ MPa]

have been characterized. For the 12PZw-PI-10, according to Ref. [2], the typical time spent associated is $\tau_{as} = 10^6$ s, the typical time spent free is $\tau_{free} = 9$ s, hence, the fraction of free arms at equilibrium is $1 - \phi \approx 10^{-5}$ according to our Equation (10). From these values we know that this system is located in the part A of Figure 3 because $\tau_{free} \ll \tau_d \ll \tau_{as}$.

Therefore, the relaxation peak for the population of stars with stickers is expected to occur in the range $10^{-9} < [\tau_d/(1-\phi)]^{-1} < 10^{-7}$ rad/s. We present in Figure 5 the predictions of our model for three different orientation relaxation times $\tau_d = 10^2$, 10^3, and 10^4 s, and the above mentioned values for τ_{as} and τ_{free}. The loss modulus exhibits three "single" peaks of relaxation centered at $[(1-\phi)/\tau_d]$ rad/s, thin colored lines. We can also include a fraction (13% as reported by Ref. [2]) of "non-active arm" to our model, i.e. non-functionalized arms, corresponding to the sticker being "always free" in our model: the thick dot-dashed lines Figure 5. The loss modulus has now an additional peak corresponding to the relaxation of the "non-active arms".

It is evident that our simple model captures with success the height of the different loss

modulus peaks, and the characteristic relaxation events. For each considered τ_d, we obtain two narrow peaks. As we vary τ_d across the considered range (10^2 to 10^4), the left peak spans the observed range of relaxation frequencies for the attached arms, whilst the right-hand peak spans the observed range of relaxation frequencies for the non-sticky arms. Hence, in the linear regime, our model with a single orientation relaxation can be considered a simplified version of the more elaborate linear rheology model of van Ruymbeke and co-workers [2]. One effect captured by their more refined model is the shape of the relaxation peaks due to dynamic dilution as the different part of the star arms relax. It is impossible to capture such details in our single mode model!

Note that our model does not predict the high-frequency regime where the Rouse modes within the tube are dominant i.e. $G', G'' \propto \omega^{1/2}$.

IV. PREDICTIONS OF THE MODEL: NON-LINEAR REGIME

A. Presentation of the parameter space

In order to explore the rheological response of the non-linear regime of the set of equations presented in Section II, we explore the shear and elongation predictions of start-up flows.

In contrast to the broad spectrum of star-arm orientation relaxation times, the non-linear regime is characterized by a single stretch relaxation time, τ_s. With the same approach as in Section III, we have selected three parameters of our model to explore. We present our predictions for the stress growth coefficient (viscosity), the average stretch of the attached and detached populations, as well as the fraction of the attached stickers, (respectively λ_A, λ_D, and f) as a function of time for different sets of the parameters τ_{as}, τ_{free}, and τ_s, in shear and elongation flows.

In Figure 6, boundaries between different regions correspond to places in parameter space where critical rates are equal. Qualitative changes in non-linear response are observed when the critical flow rates are exceeded.

There are also critical flow rates corresponding to orientation relaxation, however, we are exploring flow rates, κ, such that $\kappa\tau_d \gg 1$ – where $\kappa \equiv \dot{\gamma}$ or $\dot{\varepsilon}$, in shear or elongation respectively. We consider that the tubes are all oriented as we perform the simulations in the regime of high Weissenberg number related to the tube orientation relaxation time.

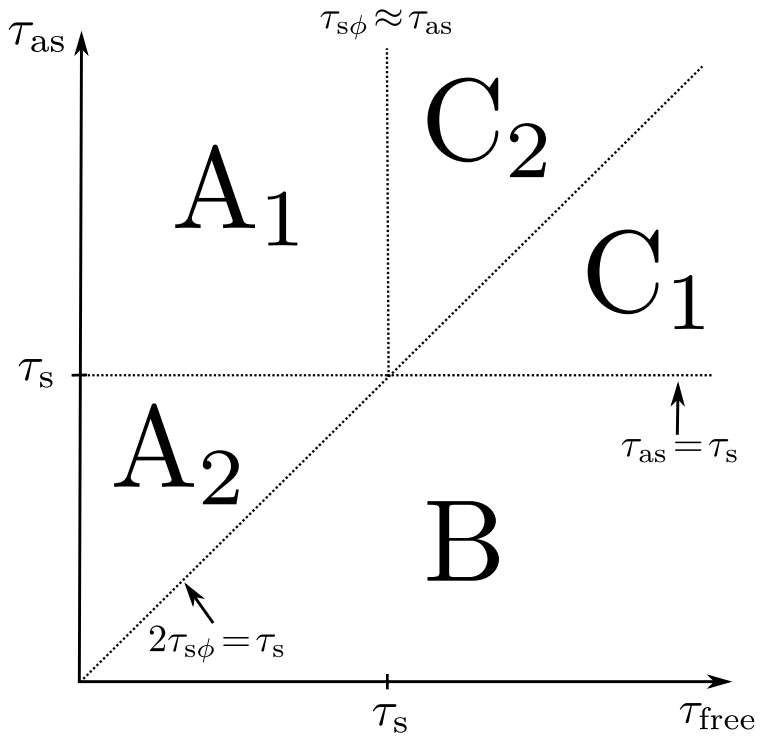

FIG. 6. Parameter map showing the different regions delimited by the lines where the critical timescales, τ_{as}, τ_{s}, and $\tau_{\mathrm{s}\phi}$ meet.

Hence, all flow rates considered are above critical orientation rates. At lowest flow rates we get thinning behavior in both shear and extension, i.e. the response follows the linear envelope up to strain of order 1, followed by a plateau in extension, or a weak overshoot and steady state in shear (similar to linear polymers in the regime $\tau_{\mathrm{d}}^{-1} < \dot{\gamma} < \tau_{\mathrm{s}}^{-1}$). At low flow rates, no stretching is seen ($\lambda \approx \lambda_{\mathrm{D}} \approx 1$) and the fraction of attached stickers stays at its initial value ($f(t) \approx \phi$).

At higher flow rates, stronger non-linear behaviors are apparent, and in different regions of parameter space, the critical rates are encountered in different orders. In particular, three timescales seem important: τ_{as}, τ_{s}, and $\tau_{\mathrm{s}\phi} = \tau_{\mathrm{s}}/(1-\phi)$. The latter is the renormalized stretch relaxation time that arises from the blinking (attached-detached) of the sticker when $\tau_{\mathrm{free}} \ll \tau_{\mathrm{as}} \ll \tau_{\mathrm{s}}$. In that regime, most of the stickers are initially attached. When the arm is stretched and that the sticker is forced to detach, it stays free, on average, for a time τ_{free} (much shorter than τ_{s}), which means that the arms are not able to relax all stretch in one detachment event. Stretch relaxation occurs only when the sticker is free, and this

is the case for a fraction $(1-\phi)$ of the time. Hence, similarly to renormalization of the orientation relaxation time, $\tau_{\rm d}$, in the linear regime seen in Section III, this leads to a renormalized *stretch* relaxation time $\tau_{{\rm s}\phi} = \tau_{\rm s}/(1-\phi)$, as defined below. This renormalized stretch relaxation time plays a role in the regions A_1 and A_2 Figure 6, similarly to the linear regime described in Section III. Note that in regions B and C_1, $\tau_{{\rm s}\phi} \approx \tau_{\rm s}$ because $\phi \ll 1$.
A time scale, $\tau_{\rm free}$, seems less important. Then we can divide space up into different regions A_1, A_2, B, C_1, and C_2 as shown in Figure 6.

The region A_1 is where $\tau_{\rm s} \ll \tau_{\rm as} \ll \tau_{{\rm s}\phi}$, which corresponds to $\tau_{\rm free} \ll \tau_{\rm s}$ and $\tau_{\rm s} \ll \tau_{\rm as}$. The transition from A_1 to C is when $\tau_{{\rm s}\phi} \approx \tau_{\rm as}$ or, equivalently, $\tau_{\rm free} \approx \tau_{\rm as}$. In this region, stickers like to stay associated and free stickers have a short lifetime compared to the stretch relaxation time.

Region A_2 is when $\tau_{\rm as} \ll \tau_{\rm s} \ll \tau_{{\rm s}\phi}$ i.e. $\tau_{\rm free} \ll \tau_{\rm as}$ and $\tau_{\rm as} \ll \tau_{\rm s}$. It is a region where the stickers attach and detach rapidly with respect to the stretch relaxation time, but are initially mostly attached $(1-\phi \ll 1)$.
The transition from A_1 to A_2 is when $\tau_{\rm as} = \tau_{\rm s}$. The only change between region A_1 and A_2 is the second critical rate encountered on increasing flow rate. Region B is where $\tau_{\rm as} \ll \tau_{{\rm s}\phi} \approx \tau_{\rm s}$, which corresponds to $\tau_{\rm s} \ll \tau_{\rm free}$ and $\tau_{\rm as} \ll \tau_{\rm s}$. The transition from A_2 to B is where $\phi \approx 1/2$. It is a region where the stickers are initially mostly free and they do not like to stay associated. It is a "non-sticky" region. Indeed, our predictions of the shear stress growth coefficient, η^+, in this regime are consistent with shear experiments on *non-telechelic* entangled star polymers [41].

Region C_1 is where $\tau_{\rm s} \approx \tau_{{\rm s}\phi} \ll \tau_{\rm as}$, which corresponds to $\tau_{\rm s} \ll \tau_{\rm as} \ll \tau_{\rm free}$. When attached, the stickers stay attached a long time compared to the stretch relaxation time, but most of the stickers are initially detached because ϕ is close to zero. The transition from B to C_1 is when $\tau_{\rm as} \approx \tau_{\rm s}$.

Finally, region C_2 is where $\tau_{\rm s} \ll \tau_{{\rm s}\phi} \ll \tau_{\rm as}$, which corresponds to $\tau_{\rm s} \ll \tau_{\rm free} \ll \tau_{\rm as}$. When attached, the stickers stay attached a long time compared to the stretch relaxation time, but most of the stickers are initially attached because ϕ is close to one. The transition from C_1 to C_2 is when $\tau_{\rm as} = \tau_{\rm free}$, or equivalently $\phi = 1/2$.

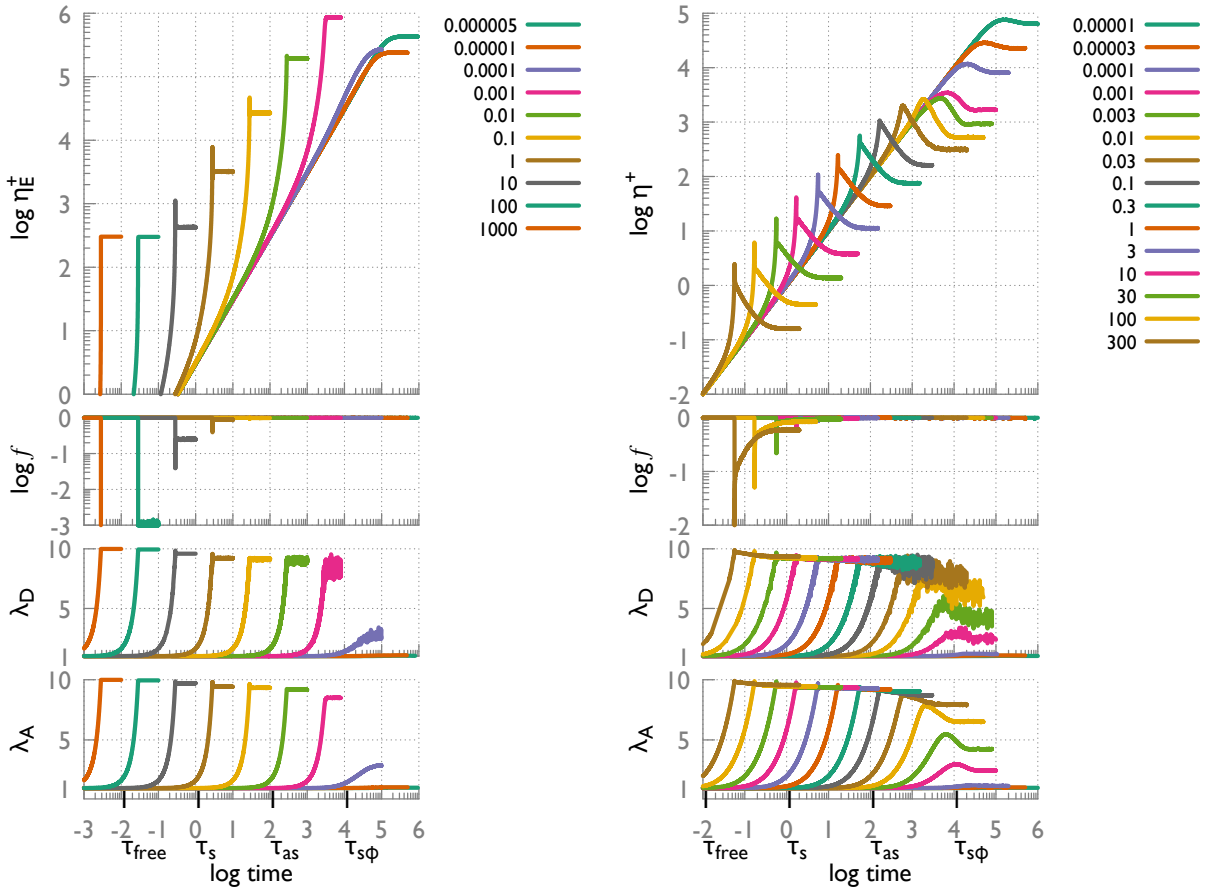

(a) Elongation

(b) Shear

FIG. 7. Stochastic model predictions for region A_1 in the non-linear regime. We present the values, as a function of time, of the fraction of attached chains, f, the stretch of the attached chains λ_A and stretch of the detached chains λ_D, and stress growth coefficients, η_E^+ and η^+, for uniaxial extension (left), and step rate (right) respectively. Parameters are $\tau_{free} = 10^{-2}$, $\tau_{as} = 10^2$, $\tau_s = 1$, $\tau_d = 10^6$ $\lambda_{max} = 10$.

In regions A_1, A_2, and B, $\tau_{as} \ll \tau_{s\phi}$. This condition ensures that interchange between the attached and detached population keeps the stretch of the attached and detached population approximately equal: $\lambda_A \approx \lambda_D$. On the other hand, the regions C_1 and C_2 have $\tau_{s\phi} \ll \tau_{as}$, which implies a separation between populations of attached and detached chains.

Indeed, when the flow rate exceeds the inverse of $\tau_{s\phi}$ in regions A_1, A_2, and C_2 or τ_s in regions B and C_1, we expect to see an onset of stretch of the attached *and* detached chains.

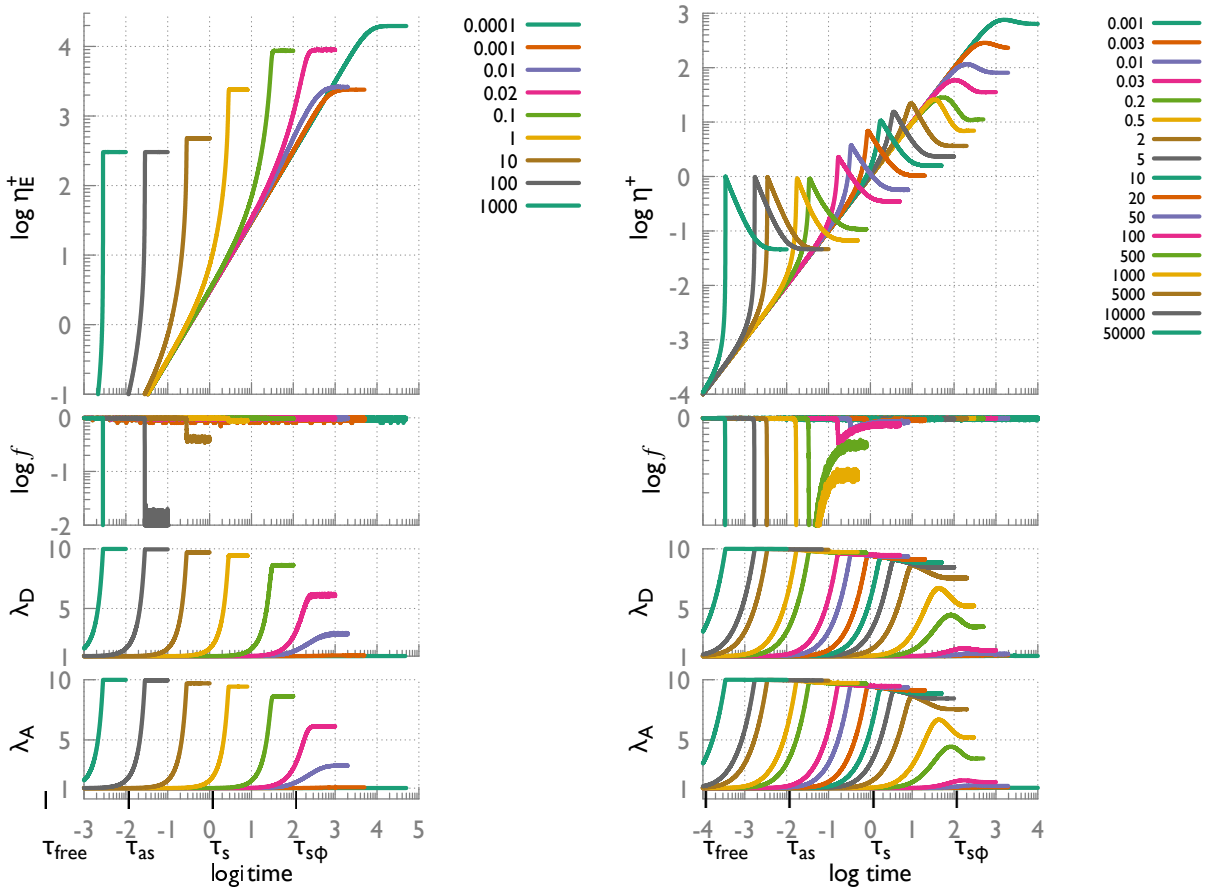

(a) Elongation

(b) Shear

FIG. 8. Stochastic model predictions for region A_2 in the non-linear regime. We present the values, as a function of time, of the fraction of attached chains, f, the stretch of the attached chains λ_A and stretch of the detached chains λ_D, and stress growth coefficients, η_E^+ and η^+, for uniaxial extension (left), and step rate (right) respectively. Parameters are $\tau_{free} = 10^{-4}$, $\tau_{as} = 10^{-2}$, $\tau_s = 1$, $\tau_d = 10^6$ $\lambda_{max} = 10$.

Additionally, if the flow rate exceeds the inverse of τ_{as} before those, as is it the case in regions C_1, and C_2 where $\tau_{s\phi} \ll \tau_{as}$, we expect *only* the attached chains to stretch, but not the detached chains. However, because the attached chain will eventually detach due to Equation (15), it will consequently increase the average stretch of the detached chains. The bottom graphs of Figures 7–11, in shear and elongation, where we plotted the average values of the stretch for the attached chains and detached chains as a function of time, support that statement..

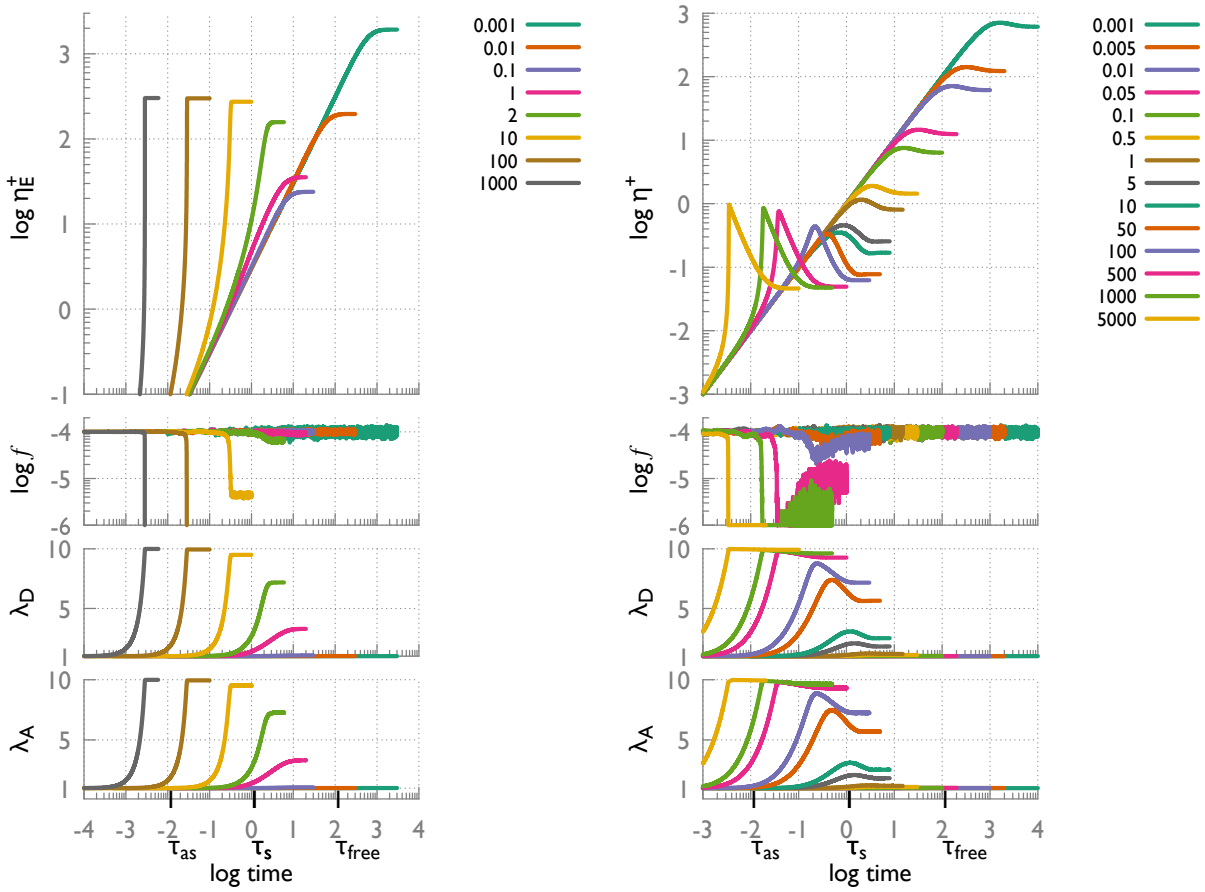

(a) Elongation

(b) Shear

FIG. 9. Stochastic model predictions for region B in the non-linear regime. We present the values, as a function of time, of the fraction of attached chains, f, the stretch of the attached chains λ_A and stretch of the detached chains λ_D, and stress growth coefficients, η_E^+ and η^+, for uniaxial extension (left), and step rate (right) respectively. Parameters are $\tau_{free} = 10^2$, $\tau_{as} = 10^{-2}$, $\tau_s = 1$, $\tau_d = 10^6$ $\lambda_{max} = 10$.

In the following sections, to explore the map Figure 6, we will choose "extreme" parameters to separate out timescales by orders of magnitude and clearly delineate different typical responses of the material.

B. Elongation

On the left parts of the Figures 7–11, we present the predictions of our model in the regions A_1, A_2, B, C_1, and C_2, respectively, for the logarithms of the tensile stress growth

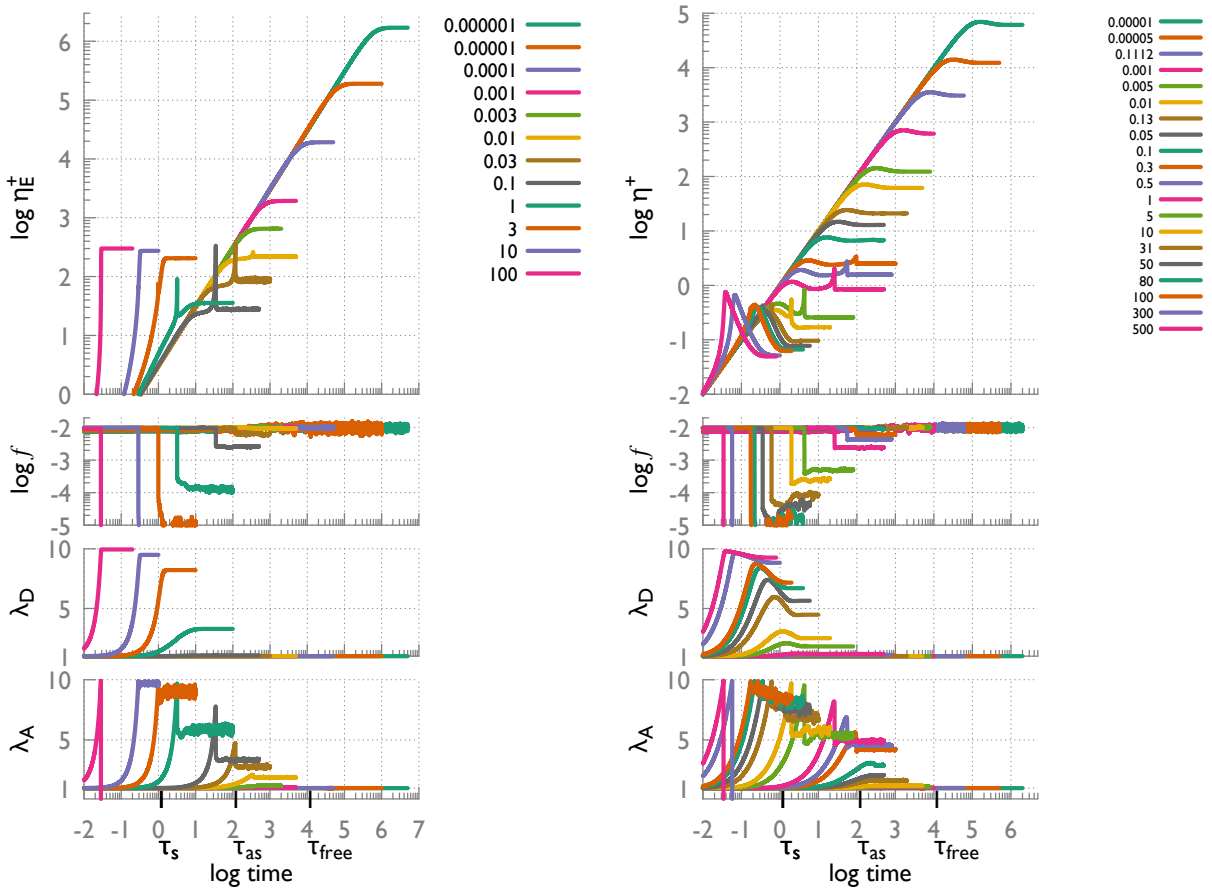

(a) Elongation

(b) Shear

FIG. 10. Stochastic model predictions for region C_1 in the non-linear regime. We present the values, as a function of time, of the fraction of attached chains, f, the stretch of the attached chains λ_A and stretch of the detached chains λ_D, and stress growth coefficients, η_E^+ and η^+, for uniaxial extension (left), and step rate (right) respectively. Parameters are $\tau_{free} = 10^4$, $\tau_{as} = 10^2$, $\tau_s = 1$, $\tau_d = 10^6$ $\lambda_{max} = 10$.

coefficient (sometimes known as extensional viscosity), $\eta_E^+(t, \dot{\varepsilon})$, the fraction of attached chains f, and the stretch of the attached and detached chains, λ_A and λ_D, as a function of time.

In all five regions, the tensile stress growth coefficient follows the linear visco-elastic envelope (LVE) up to strain of order 1, i.e. $\dot{\varepsilon}t \approx 1$, where $\dot{\varepsilon}$ is the Hencky strain rate (elongation rate), the chains are not stretched ($\lambda_A \approx \lambda_D \approx 1$) and the fraction of attached chains is not modified, $f \approx \phi$. For $\dot{\varepsilon}t > 1$, the behavior depends on how $\dot{\varepsilon}$ compares with the different

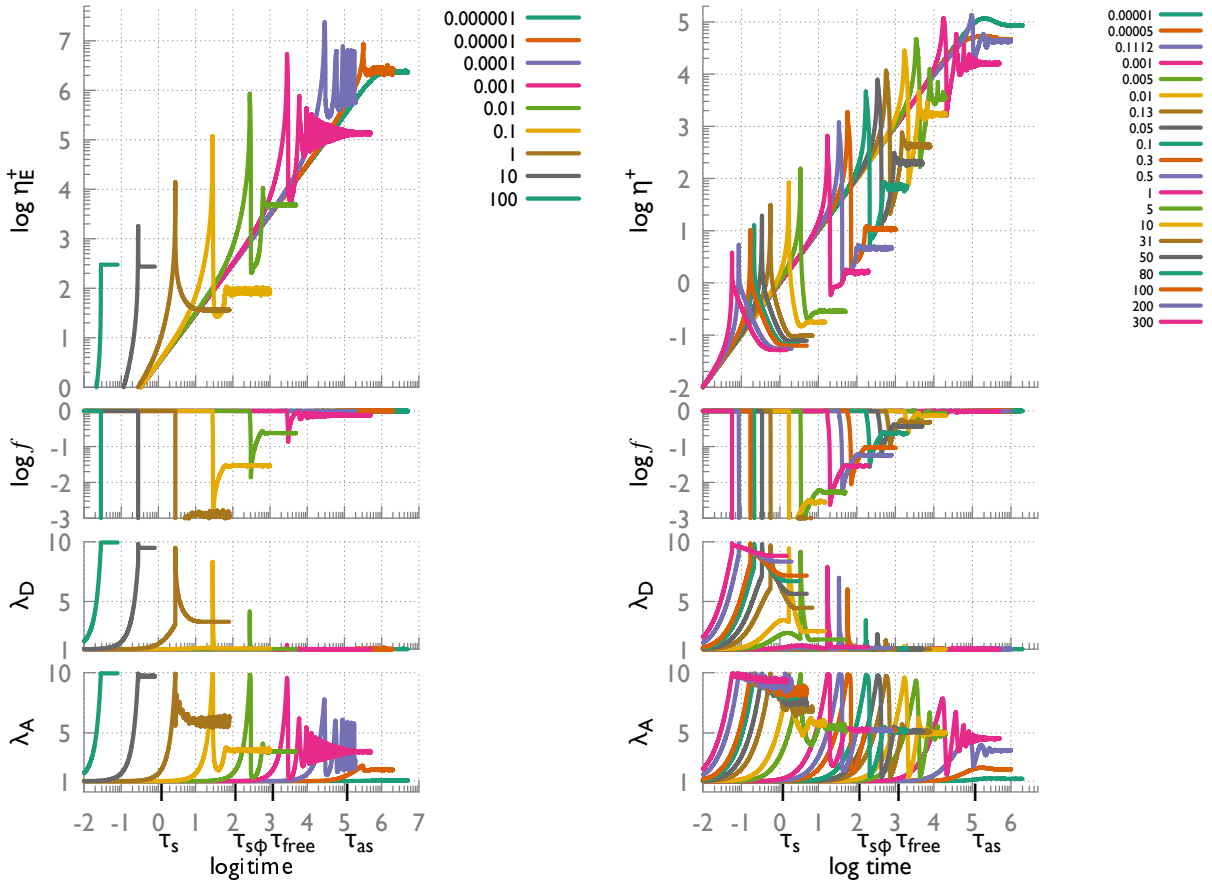

(a) Elongation

(b) Shear

FIG. 11. Stochastic model predictions for region C_2 in the non-linear regime. We present the values, as a function of time, of the fraction of attached chains, f, the stretch of the attached chains λ_A and stretch of the detached chains λ_D, and stress growth coefficients, η_E^+ and η^+, for uniaxial extension (left), and step rate (right) respectively. Parameters are $\tau_{free} = 10^3$, $\tau_{as} = 10^5$, $\tau_s = 1$, $\tau_d = 10^6$ $\lambda_{max} = 10$.

timescales.

In regions A_1 and A_2 Figure 6, the stretch relaxation time is rescaled similarly to the linear regime, Section III. The stretch is able to relax mainly when the stickers are free and this is the case for a fraction $1-\phi$ of arms. Over a time t, the arm is effectively detached for a time $t/(1-\phi)$. Thus, the effective stretch relaxation time is longer than τ_s by a factor $1-\phi$. The stickers are blinking between attached and detached states in regions A_1 and A_2. When $\dot{\varepsilon} < \tau_{s\phi}^{-1} = [\tau_s/(1-\phi)]^{-1}$, the viscosity reaches a steady state plateau, $\lambda_A \approx \lambda_D \approx 1$,

and $f \approx \phi$. If $\dot{\varepsilon} > \tau_{s\phi}$, we observe elongation hardening due to chain stretching, followed by a steady state plateau.

In region A_1, Figure 7 left, at intermediate elongation rates when $\tau_{as}^{-1} < \dot{\varepsilon} < \tau_s^{-1}$, small overshoots appear: the chains are stretched and reach the maximum extensibility because the flow rate is faster than the average time needed for a sticker to detach: $\tau_{as}^{-1} < \dot{\varepsilon}$. That triggers the detachment of stickers, as confirmed by the undershoot of f, and therefore immediate relaxation of the stretch of the arm because the stretch relaxation time is faster than the flow: $\dot{\varepsilon} < \tau_s^{-1}$. However, the time the sticker will spend free is small compared to the stretch relaxation time, hence, only a fraction of stress can be relaxed – in contrast with findings in region C_2.
As expected, these small overshoots in η_E^+ and undershoots in f, are not seen in the region A_2, Figure 8 left, as $\tau_{as} \ll \tau_s$ implies that increasing elongation rates will exceed τ_s^{-1} before τ_{as}^{-1}. Therefore, when $\tau_{as}^{-1} < \dot{\varepsilon}$, the maximum extensibility is reached and chains are forced to detach but they cannot fully relax the stretch as the flow rate is faster than the stretch relaxation time.

In region B Figure 6, we are in a non-sticky regime because most of the stickers are free and the lifetime of an associated sticker is short. As before, in Figure 9 left, the viscosity follows the LVE up to strain of order 1. If $\dot{\varepsilon} < \tau_s^{-1}$, η_E^+ reaches a steady state plateau. If $\dot{\varepsilon} > \tau_s^{-1}$ we see elongation hardening due to chain stretching, followed by a steady state plateau.

In regions C_1 and C_2 Figure 6, there is no rescaling of the stretch relaxation time because the dynamic of association/disassociation of the stickers is slow compared to the stretch relaxation, i.e. there is no renormalization due to the blinking phenomena seen in regions A_1 and A_2. Thus, $\tau_{s\phi}$ is irrelevant there.

In region C_2, Figure 11 left, we observe elongation hardening as soon as the flow rate exceeds the inverse association time, $\dot{\varepsilon} > \tau_{as}^{-1}$. Indeed, ϕ being close to unity, almost all chains are initially attached and they will stay attached long enough to be stretched by the flow until the chains reach their maximal extensibility where they are forced to detach. On the other hand, the detached chains are not stretched at this point. The dramatic drop in viscosity is due to the fast relaxation of the arms stretch immediately following the detachment of the stickers. At moderately high flow rates, when $\tau_{as}^{-1} < \dot{\varepsilon} < \tau_s^{-1}$, the chains can "fully" relax their stretch before the stickers re-attach and stretch the arm again.

This cycle of attachment-stretch/detachment-relaxation is responsible for the undershoot and oscillation in viscosity seen at intermediate elongation rate. At high elongation rates, when $\dot{\varepsilon} > \tau_s^{-1}$, the chains that are forced to detach are only able to partially relax their stretch before the stickers re-attach, which produces a smooth transition towards the steady state with no undershoot or oscillation. Indeed, when $\dot{\varepsilon} > \tau_s^{-1}$, the detached chains also start to stretch.

In region C_1, Figure 10 left, we observe something intermediate between the regions B and C_2. At small elongation rate, $\dot{\varepsilon} < \tau_s^{-1}$, η_E^+ follows the LVE and reaches a steady state plateau that is below the LVE, similar to region B. Additionally, at intermediate elongation rates, $\tau_{as}^{-1} < \dot{\varepsilon} < \tau_s^{-1}$, sharp spikes of the tensile stress growth coefficient are visible, similar to region C_2. These small spikes are the result of the few initially attached chains (recall that ϕ is close to zero in region C_1) that stretch until they detach, and because the flow is "slower" than stretch relaxation time, they can fully relax their stretch. Indeed, at these elongation rates, the detached chains are not stretched. At high flow rates, $\tau_s^{-1} < \dot{\varepsilon}$, the chains that are forced to detach are only able to partially relax their stretch as they are being dragged by the flow: the detached chains are stretching too. On increasing ϕ, the spikes are more pronounced. The transition from C_1 to C_2 is when $\phi \approx 1/2$.

C. Shear

On the right parts of the Figures 7–11, we present the predictions of our model in the regions A_1, A_2, B, C_1, and C_2, respectively, for the logarithms of the shear stress growth coefficient (sometimes known as shear viscosity), $\eta^+(t, \dot{\gamma})$, the fraction of attached chains f, and the stretch of the attached and detached chains, λ_A and λ_D, as a function of time.
As in elongation, up to a strain of order 1, the viscosity follows the LVE, the chains are not stretched ($\lambda_A \approx \lambda_D \approx 1$) and the fraction of attached chains is not modified, $f \approx \phi$. The subsequent behavior strongly depends on the different parameters and the applied shear rate. We detail below the predictions in the different regions.

1. *Regions A_1, A_2, B*

(i) When the shear rate is smaller than the inverse of the effective stretch relaxation time, $\tau_{s\phi} = \tau_s/(1-\phi)$, for regions A_1 and A_2, or smaller than the stretch relaxation time τ_s for region B, the viscosity shows a mild overshoot before reaching the steady state. This mild overshoot under the LVE has been observed experimentally for *non-telechelic* entangled stars [41]. Indeed, at low shear rates, the system is not aware of the stickers.

(ii) As the shear rate crosses the above mentioned timescales, τ_s or $\tau_{s\phi}$, the stress overshoot becomes more pronounced and its height increases. This is typical for entangled linear chains in the chain stretching regime. The response remains below the LVE, so still in the shear thinning regime. We also start to see the onset of stretch of the attached and detached chains.

(iii) We observe in Figures 7–9 right, that, above a second critical shear rate, shear hardening occurs, i.e. η^+ goes above the LVE.

In regions A_1, A_2, and B, we have found empirically that this critical shear rate above which hardening is seen, $\dot{\gamma}_c^{\text{hard}}$, depends on the maximal stretch $\lambda_{\max}$, on the stretch relaxation time τ_s, and the fraction of associated arms at equilibrium, ϕ, as

$$\dot{\gamma}_c^{\text{hard}} = \left[\frac{\tau_s}{6\lambda_{\max}(1-\phi)}\right]^{-1}. \tag{21}$$

We note that this hardening is a feature of the Rolie-Poly model with finite extensibility, i.e. if ϕ is set to zero, there remains a critical rate in Equation (21) above which shear hardening is seen.

In addition, we observe in region A_1 that, at intermediate to high shear rates, sharp peaks in viscosity appear. Similarly to the elongation case, at moderately high shear rates, $\tau_{as}^{-1} < \dot{\gamma}$, the chains are stretched and reach the maximum extensibility, as $\tau_{as}^{-1} < \dot{\gamma}$, which triggers the detachment of stickers and therefore immediate relaxation of the stretch of the arm because $\lambda_D < \lambda_A$. On the other hand, in region A_2, $\lambda_A \approx \lambda_D$ so the stress does not relax as fast. Hence, we do not see the sharp decrease in viscosity at high shear rates.

2. *Regions C*

In region C_2, Figure 11 right, the critical shear rate at which shear hardening occurs is $\dot{\gamma}_c^{\text{hard}} = \tau_{as}^{-1}$. Note that in region C_2, the regime (ii) above is not seen due to the high value of

τ_{as}. In addition, when the shear rate exceeds τ_{as}^{-1}, the associated arms are strongly stretched until they reach the maximal stretch ratio. This corresponds to the onset of shear hardening. Then the strongly stretched arms are forced to detach and will stay detached during τ_{free} in average. Because $\tau_s \ll \tau_{free}$, the detached arms can fully relax before getting reattached ($\lambda_D < \lambda_A$). This fast relaxation is responsible for the undershoots visible at intermediate shear rates. At higher shear rates, $\dot{\gamma} > \tau_s^{-1}$, the detached arms can only partially relax as they are dragged by the flow, which produces a smooth transition towards the steady state with no undershoot or oscillation ($\lambda_D \approx \lambda_A$).

In region C_1, Figure 10 right, we observe a behavior intermediate between the regions B and C_2. Changes in the shape of the stress growth coefficient are seen when the above mentioned – in (i), (ii), and (iii) – critical (inverse) times scales are exceeded by the flow rate, i.e. τ_s^{-1} and $\dot{\gamma}_c^{hard}$. Additionally, small spikes appear at intermediate flow rates, when $\tau_{as}^{-1} < \dot{\gamma} < \tau_s^{-1}$, due to the same mechanism described above for the region C_2. However, these spikes are of small amplitude because the initial fraction of attached chain is close to zero ($\phi \approx 0$). On increasing ϕ, these spikes are more pronounced.

V. PRE-AVERAGED MODEL

A. Motivations

The stochastic model just presented is in good qualitative agreement with experimental linear rheology data; the reasons listed at the end of Section III C explain the discrepancies in the low frequency region (due to dilution effects) and in the plateau region for G" (the spectrum of orientation relaxation times is not accounted for in our simple model). To our knowledge, no non-linear rheology data on entangled telechelic star polymers have been published.

The stochastic model predicts a wide range of interesting non-linear behavior as parameters are varied e.g. shear hardening, sharp stress peaks and and a non-monotonic constitutive curve (see Figure 17) which we anticipate may be exhibited in real materials. Given this, there is potential interest in using the constitutive model in computations for more complex flows. Such computations could, for example, allow qualitative investigation of the relationship between the predicted non-linear viscoelasticity and flow phenomena such as transient

or steady state shear banding. Our toy model might also be applicable at the same level as the multimode pom-pom model for branched polymers [13], in which the model parameters are usually adjusted freely so as to match available linear and non-linear rheology, which can then serve to make reasonably accurate predictions in non-viscometric flows.

We may also note that much of the interesting non-linear behaviour we predict arises from interaction of the flow and sticker timescales with the stretch relaxation time τ_s of the stars. Our toy model is not designed to capture the full spectrum of orientation relaxation times for a "real" star arm, applicable to linear rheology. However, star polymers are expected to possess a single dominant stretch relaxation time: in this respect our model is quite close to reality and we may anticipate that in this sense our non-linear predictions might be more accurate than the linear ones, especially at high flow rates in the strongly non-linear regime!

However, the model we have presented so far is not very efficient for numerical computation in complex flows such as shear banding calculations because of the cost of solving stochastic equations for many arms. Given this, we develop, in this section, a pre-averaged version of the stochastic model, which is far less computationally costly and retains most of the features of the stochastic model. We get rid of the stochastic nature of the model by pre-averaging the contributions to the stress of the attached and detached populations. The outcome is a scalar differential equation for the time-dependent fraction of attached chains, $f(t)$, and two tensorial equations for the conformational average of the associated and dissociated chains, $\underline{\underline{\boldsymbol{Q}}}_{\mathrm{A}}(t)$ and $\underline{\underline{\boldsymbol{Q}}}_{\mathrm{D}}(t)$, similar to Refs. [5, 42].

B. Assumptions of the model

The evolution equation of the fraction of attached chains, f, is constrained by detailed balance, and reads

$$\frac{\mathrm{d}f}{\mathrm{d}t} = \frac{1}{N}\frac{\mathrm{d}n_{\mathrm{A}}}{\mathrm{d}t} = (1 - f(t))r_{\mathrm{free}\to\mathrm{as}} - f(t)r_{\mathrm{as}\to\mathrm{free}}(\lambda_{\mathrm{A}}) \tag{22}$$

where n_{A} is the instant number of associated chain, N is the total number of chains, the rate of dissociation and association $r_{\mathrm{free}\to\mathrm{as}}$, and $r_{\mathrm{as}\to\mathrm{free}}(\lambda_{\mathrm{A}})$ are defined by Equations (7) and (15) respectively, and the stretch ratio of the attached population, λ_{A}, is defined below in Equation (27).

The conformation tensor, $\underline{\underline{\boldsymbol{\tau}}}$ defined Section II B, is split up into two contributions: the associated and dissociated populations, $\underline{\underline{\boldsymbol{\tau}}}_{\mathrm{A}}$ and $\underline{\underline{\boldsymbol{\tau}}}_{\mathrm{D}}$, respectively. The time evolution of the tensor representing the associated chains, $\underline{\underline{\boldsymbol{\tau}}}_{\mathrm{A}}$, is given by Equation (17). The time evolution of the tensor representing the detached chains, $\underline{\underline{\boldsymbol{\tau}}}_{\mathrm{D}}$, is given by Equation (19).
The stress tensor, $\underline{\underline{\boldsymbol{\sigma}}}$, of the full system is then defined as the sum of the contributions of the attached and detached chains, weighted by the fraction of such chains, $f(t)$ and $1-f(t)$ respectively. Including the finite extensibility function, we obtain, in units of G,

$$\underline{\underline{\boldsymbol{\sigma}}} = f\mathrm{fene}(\lambda_{\mathrm{A}})\underline{\underline{\boldsymbol{\tau}}}_{\mathrm{A}} + (1-f)\mathrm{fene}(\lambda_{\mathrm{D}})\underline{\underline{\boldsymbol{\tau}}}_{\mathrm{D}}, \tag{23}$$

where λ_{A} and λ_{D} are the stretch ratio of the attached and detached populations and are defined below. The rest of this section aims at defining the time evolution of Equation (23) and concludes by comparing with the predictions of the stochastic model of the previous section. In deriving the pre-averaged model, one constraint upon which we insist is that attachment and detachment events, on their own, should not result in a change in stress – rather stress relaxation occurs when detached chains relax.

C. Tensor pre-averaging

We consider the two tensors, related to the stress of the attached and detached chains, defined by

$$\underline{\underline{\boldsymbol{Q}}}_{\mathrm{A}} = \mathrm{fene}\left(\lambda_{\mathrm{A}}\right)\underline{\underline{\boldsymbol{\tau}}}_{\mathrm{A}} \tag{24}$$

$$\underline{\underline{\boldsymbol{Q}}}_{\mathrm{D}} = \mathrm{fene}\left(\lambda_{\mathrm{D}}\right)\underline{\underline{\boldsymbol{\tau}}}_{\mathrm{D}}, \tag{25}$$

where $\lambda_{\mathrm{A}}^2 = \mathrm{tr}\,\underline{\underline{\boldsymbol{\tau}}}_{\mathrm{A}}/3$, and $\lambda_{\mathrm{D}}^2 = \mathrm{tr}\,\underline{\underline{\boldsymbol{\tau}}}_{\mathrm{D}}/3$ are the pre-averaged stretch ratio of, respectively, the attached and detached populations, such that the total stress in units of G is

$$\underline{\underline{\boldsymbol{\sigma}}} = f\underline{\underline{\boldsymbol{Q}}}_{\mathrm{A}} + (1-f)\underline{\underline{\boldsymbol{Q}}}_{\mathrm{D}}. \tag{26}$$

We can express the two stretch ratios as a function of the traces of the tensors $\underline{\underline{\boldsymbol{Q}}}_{\mathrm{A}}$ and $\underline{\underline{\boldsymbol{Q}}}_{\mathrm{D}}$. Trace of Equation (24) gives

$$\begin{aligned}
\mathrm{tr}\left(\underline{\underline{\boldsymbol{Q}}}_{\mathrm{A}}\right) &= \frac{1-\lambda_{\max}^{-2}}{1-\lambda_{\mathrm{A}}^2\lambda_{\max}^{-2}}\,\mathrm{tr}\left(\underline{\underline{\boldsymbol{\tau}}}_{\mathrm{A}}\right) \\
\left(1-\lambda_{\mathrm{A}}^2\lambda_{\max}^{-2}\right)\mathrm{tr}\left(\underline{\underline{\boldsymbol{Q}}}_{\mathrm{A}}\right) &= \left(1-\lambda_{\max}^{-2}\right)3\lambda_{\mathrm{A}}^2 \\
\lambda_{\mathrm{A}}^2 &= \frac{\lambda_{\max}^2\,\mathrm{tr}\left(\underline{\underline{\boldsymbol{Q}}}_{\mathrm{A}}\right)}{3\lambda_{\max}^2-3+\mathrm{tr}\left(\underline{\underline{\boldsymbol{Q}}}_{\mathrm{A}}\right)}.
\end{aligned} \tag{27}$$

Similarly, Equation (25) gives

$$\lambda_{\mathrm{D}}^2 = \frac{\lambda_{\max}^2\,\mathrm{tr}\left(\underline{\underline{\boldsymbol{Q}}}_{\mathrm{D}}\right)}{3\lambda_{\max}^2-3+\mathrm{tr}\left(\underline{\underline{\boldsymbol{Q}}}_{\mathrm{D}}\right)}. \tag{28}$$

We deduce the expression of the fene function depending on the tensor $\underline{\underline{\boldsymbol{Q}}}_{i}$, $i \equiv$ A or D,

$$\mathrm{fene}(\lambda_i) = \frac{3\lambda_{\max}^2-3+\mathrm{tr}\left(\underline{\underline{\boldsymbol{Q}}}_{i}\right)}{3\lambda_{\max}^2}. \tag{29}$$

We will now express the time evolution the two tensors $\underline{\underline{\boldsymbol{Q}}}_{\mathrm{A}}$ and $\underline{\underline{\boldsymbol{Q}}}_{\mathrm{D}}$. This is a two-fold process. First, we will define the exchange terms that arise from the switch between attached and detached states. Then, we define the flow contribution.

1. *Exchange terms*

The exchange term is present to ensure that the total stress remains constant when a fraction of chains detaches or attaches. The exchange term is given by writing the time increment of the quantity $f\underline{\underline{\boldsymbol{Q}}}_{\mathrm{A}}$ between the times t and $t+\Delta t$, in absence of flow or relaxation. At a time $t+\Delta t$, a fraction $\Delta t f r_{\mathrm{as}\to\mathrm{free}}(\lambda_{\mathrm{A}})$ of chains have detached, while a fraction $\Delta t(1-f)r_{\mathrm{free}\to\mathrm{as}}$ have attached. We write

$$f(t+\Delta t)\underline{\underline{\boldsymbol{Q}}}_{\mathrm{A}}(t+\Delta t) = f(t)\underline{\underline{\boldsymbol{Q}}}_{\mathrm{A}}(t) + \Delta t\left(\left(1-f(t)\right)r_{\mathrm{free}\to\mathrm{as}}\underline{\underline{\boldsymbol{Q}}}_{\mathrm{D}}(t) - f(t)r_{\mathrm{as}\to\mathrm{free}}(\lambda_{\mathrm{A}})\underline{\underline{\boldsymbol{Q}}}_{\mathrm{A}}(t)\right).$$

By rearranging the terms we obtain, in a first approximation, the exchange terms

$$\left.\frac{\mathrm{d}\underline{\underline{\boldsymbol{Q}}}_{\mathrm{A}}}{\mathrm{d}t}\right|_{\mathrm{exchange}} = r_{\mathrm{free}\to\mathrm{as}}\frac{1-f}{f}(\underline{\underline{\boldsymbol{Q}}}_{\mathrm{D}} - \underline{\underline{\boldsymbol{Q}}}_{\mathrm{A}}), \tag{30}$$

and similarly

$$\left.\frac{\mathrm{d}\underline{\underline{\boldsymbol{Q}}}_{\mathrm{D}}}{\mathrm{d}t}\right|_{\text{exchange}} = r_{\text{as}\to\text{free}}(\lambda_{\mathrm{A}})\frac{f}{1-f}(\underline{\underline{\boldsymbol{Q}}}_{\mathrm{A}} - \underline{\underline{\boldsymbol{Q}}}_{\mathrm{D}}). \tag{31}$$

One can easily verify that in the absence of flow and ignoring the orientation or stretch relaxation processes, $\frac{\mathrm{d}\sigma}{\mathrm{d}t} \equiv \frac{\mathrm{d}}{\mathrm{d}t}\left(f\underline{\underline{\boldsymbol{Q}}}_{\mathrm{A}} + (1-f)\underline{\underline{\boldsymbol{Q}}}_{\mathrm{D}}\right) = \underline{\underline{\mathbf{0}}}$. Therefore, we ensure in this way that the stress stays constant when a chain attaches or detaches.

This, in fact, is the reason for writing the dynamics in terms of $\underline{\underline{\boldsymbol{Q}}}_{\mathrm{A}}$ and $\underline{\underline{\boldsymbol{Q}}}_{\mathrm{D}}$, rather than $\underline{\underline{\boldsymbol{\tau}}}_{A}$ and $\underline{\underline{\boldsymbol{\tau}}}_{D}$

2. *Flow terms*

We now derive the flow terms using Equations (17) and (19). Using the chain rule, we take the derivative with respect to time of Equation (24), and considering Equation (29) we obtain,

$$\begin{aligned}\left.\frac{\mathrm{d}\underline{\underline{\boldsymbol{Q}}}_{\mathrm{A}}}{\mathrm{d}t}\right|_{\text{flow}} &= \underline{\underline{\boldsymbol{\tau}}}_{\mathrm{A}}\frac{\mathrm{d}}{\mathrm{d}t}\left(\frac{3\lambda_{\max}^2 - 3 + \operatorname{tr}\underline{\underline{\boldsymbol{Q}}}_{\mathrm{A}}}{3\lambda_{\max}^2}\right) + \frac{3\lambda_{\max}^2 - 3 + \operatorname{tr}\underline{\underline{\boldsymbol{Q}}}_{\mathrm{A}}}{3\lambda_{\max}^2}\frac{\mathrm{d}\underline{\underline{\boldsymbol{\tau}}}_{\mathrm{A}}}{\mathrm{d}t} \\ &= \underline{\underline{\boldsymbol{\tau}}}_{\mathrm{A}}\frac{1}{3\lambda_{\max}^2}\frac{\mathrm{d}\operatorname{tr}\underline{\underline{\boldsymbol{Q}}}_{\mathrm{A}}}{\mathrm{d}t} + \frac{3\lambda_{\max}^2 - 3 + \operatorname{tr}\underline{\underline{\boldsymbol{Q}}}_{\mathrm{A}}}{3\lambda_{\max}^2}\frac{\mathrm{d}\underline{\underline{\boldsymbol{\tau}}}_{\mathrm{A}}}{\mathrm{d}t}\end{aligned} \tag{32}$$

By taking the trace of Equation (32) and re-arranging the terms, we get

$$\frac{\mathrm{d}\operatorname{tr}\underline{\underline{\boldsymbol{Q}}}_{\mathrm{A}}}{\mathrm{d}t} = \frac{3\lambda_{\max}^2 - 3 + \operatorname{tr}\underline{\underline{\boldsymbol{Q}}}_{\mathrm{A}}}{3\lambda_{\max}^2}\frac{\mathrm{d}\operatorname{tr}\underline{\underline{\boldsymbol{\tau}}}_{\mathrm{A}}}{\mathrm{d}t}\frac{3\lambda_{\max}^2 - 3 + \operatorname{tr}\underline{\underline{\boldsymbol{Q}}}_{\mathrm{A}}}{3\lambda_{\max}^2 - 3}. \tag{33}$$

We inject the latter equation into the former to obtain

$$\left.\frac{\mathrm{d}\underline{\underline{\boldsymbol{Q}}}_{\mathrm{A}}}{\mathrm{d}t}\right|_{\text{flow}} = \frac{1}{3\lambda_{\max}^2 - 3}\operatorname{tr}\left[\underline{\underline{\boldsymbol{g}}}(\underline{\underline{\boldsymbol{Q}}}_{\mathrm{A}})\right]\underline{\underline{\boldsymbol{Q}}}_{\mathrm{A}} + \underline{\underline{\boldsymbol{g}}}(\underline{\underline{\boldsymbol{Q}}}_{\mathrm{A}}), \tag{34}$$

were we have defined a tensor function $\underline{\underline{\boldsymbol{g}}}$ as

$$\begin{aligned}\underline{\underline{\boldsymbol{g}}}(\underline{\underline{\boldsymbol{Q}}}_{\mathrm{A}}) &\equiv \frac{3\lambda_{\max}^2 - 3 + \operatorname{tr}\underline{\underline{\boldsymbol{Q}}}_{\mathrm{A}}}{3\lambda_{\max}^2}\frac{\mathrm{d}\underline{\underline{\boldsymbol{\tau}}}_{\mathrm{A}}}{\mathrm{d}t} \\ &= \text{fene}(\lambda_{\mathrm{A}})\frac{\mathrm{d}\underline{\underline{\boldsymbol{\tau}}}_{\mathrm{A}}}{\mathrm{d}t}.\end{aligned} \tag{35}$$

Recall that the evolution of $\underline{\underline{\boldsymbol{\tau}}}_{\mathrm{A}}$ is defined by Equation (17), therefore we write

$$\begin{cases}\left.\dfrac{\mathrm{d}\underline{\underline{\boldsymbol{Q}}}_{\mathrm{A}}}{\mathrm{d}t}\right|_{\text{flow}} = \underline{\underline{\boldsymbol{g}}}(\underline{\underline{\boldsymbol{Q}}}_{\mathrm{A}}) + \dfrac{1}{3\lambda_{\max}^2 - 3}\operatorname{tr}[\underline{\underline{\boldsymbol{g}}}(\underline{\underline{\boldsymbol{Q}}}_{\mathrm{A}})]\underline{\underline{\boldsymbol{Q}}}_{\mathrm{A}} \\ \underline{\underline{\boldsymbol{g}}}(\underline{\underline{\boldsymbol{Q}}}_{\mathrm{A}}) \equiv \underline{\underline{\boldsymbol{\kappa}}}\cdot\underline{\underline{\boldsymbol{Q}}}_{\mathrm{A}} + \underline{\underline{\boldsymbol{Q}}}_{\mathrm{A}}\cdot\underline{\underline{\boldsymbol{\kappa}}}^{\mathrm{T}} - 2\beta\tilde{\nu}\lambda_{\mathrm{A}}^{-1}\left(\underline{\underline{\boldsymbol{Q}}}_{\mathrm{A}} - \text{fene}(\lambda_{\mathrm{A}})\underline{\underline{\boldsymbol{I}}}\right)\end{cases} \tag{36}$$

The same strategy leads to

$$\begin{cases} \left.\dfrac{\mathrm{d}\underline{\underline{\boldsymbol{Q}}}_{\mathrm{D}}}{\mathrm{d}t}\right|_{\mathrm{flow}} &= \underline{\underline{\boldsymbol{h}}}(\underline{\underline{\boldsymbol{Q}}}_{\mathrm{D}}) + \dfrac{1}{3\lambda_{\mathrm{max}}^2 - 3}\,\mathrm{tr}[\underline{\underline{\boldsymbol{h}}}(\underline{\underline{\boldsymbol{Q}}}_{\mathrm{D}})]\underline{\underline{\boldsymbol{Q}}}_{\mathrm{D}} \\ \underline{\underline{\boldsymbol{h}}}(\underline{\underline{\boldsymbol{Q}}}_{\mathrm{D}}) &\equiv \underline{\underline{\boldsymbol{\kappa}}}\cdot\underline{\underline{\boldsymbol{Q}}}_{\mathrm{D}} + \underline{\underline{\boldsymbol{Q}}}_{\mathrm{D}}\cdot\underline{\underline{\boldsymbol{\kappa}}}^{\mathrm{T}} - 2\beta\tilde{\nu}\lambda_{\mathrm{D}}^{-1}\left(\underline{\underline{\boldsymbol{Q}}}_{\mathrm{D}} - \mathrm{fene}(\lambda_{\mathrm{D}})\underline{\underline{\boldsymbol{I}}}\right) \\ & \quad -\dfrac{1}{\tau_{\mathrm{d}}}\left(\underline{\underline{\boldsymbol{Q}}}_{\mathrm{D}} - \mathrm{fene}(\lambda_{\mathrm{D}})\underline{\underline{\boldsymbol{I}}}\right) - \dfrac{2(1-\lambda_{\mathrm{D}}^{-1})}{\tau_{\mathrm{s}}}\mathrm{fene}(\lambda_{\mathrm{D}})\underline{\underline{\boldsymbol{Q}}}_{\mathrm{D}} \end{cases} \tag{37}$$

where the stretches λ_{A} and λ_{D} are defined as a function of $\underline{\underline{\boldsymbol{Q}}}_{\mathrm{A}}$ and $\underline{\underline{\boldsymbol{Q}}}_{\mathrm{D}}$ respectively in Equations (27) and (28), and, similarly to Equation (35), we have defined the tensor function $\underline{\underline{\boldsymbol{h}}}(\underline{\underline{\boldsymbol{Q}}}_{\mathrm{D}}) \equiv \mathrm{fene}(\lambda_{\mathrm{D}})\mathrm{d}\underline{\underline{\boldsymbol{\tau}}}_{\mathrm{D}}/\mathrm{d}t$, where $\mathrm{d}\underline{\underline{\boldsymbol{\tau}}}_{\mathrm{D}}/\mathrm{d}t$ is defined by Equation (19).
Note that the CCR rate, $\tilde{\nu}$, in the pre-averaged equations needs to be defined. This is the aim of the following section.

D. Pre-averaged CCR rate

For the pre-averaged model, we could define a CCR rate, $\tilde{\nu}$, that is equivalent to CCR rate defined in Equation (6), and would be

$$\tilde{\nu} = (1-f)\frac{1-\lambda_{\mathrm{D}}^{-1}}{\tau_{\mathrm{s}}}\mathrm{fene}(\lambda_{\mathrm{D}}). \tag{38}$$

The way the pre-averaging is done in the previous section, using the tensors $\underline{\underline{\boldsymbol{Q}}}_{\mathrm{A}}$ and $\underline{\underline{\boldsymbol{Q}}}_{\mathrm{D}}$, ensures that the total stress is conserved during attachment and detachment events. However, due to the non-linear relation between stress and stretch, the pre-averaged stretches are not conserved during attachment and detachment events. Hence, the CCR rate – that depends on the pre-averaged stretch λ_{D} – is incorrect if defined as in Equation (38). Indeed, we have compared CCR rates of the stochastic model (Equation (6)) with that of the above equation: the latter is higher, especially after the detachment events where the sharp drop in the stress growth coefficient occurs (see Sections IV B and IV C). As a consequence of using Equation (38), the predictions of the stress growth coefficient are qualitatively different (higher) as compared to the stochastic model.
Consequently, we introduce a new stretch variable, $\lambda_{\mathrm{D,eq}}$, for which the only purpose is to compute the CCR rate. The time evolution of the new pre-averaged stretch, $\lambda_{\mathrm{D,eq}}$, reads

$$\frac{\mathrm{d}\lambda_{\mathrm{D,eq}}}{\mathrm{d}t} = (\underline{\underline{\boldsymbol{\kappa}}} : \underline{\underline{\boldsymbol{S}}}_{\mathrm{D}})\lambda_{\mathrm{D,eq}} - \frac{\lambda_{\mathrm{D,eq}}-1}{\tau_{\mathrm{s}}}\mathrm{fene}(\lambda_{\mathrm{D,eq}}) + f r_{\mathrm{as}\to\mathrm{free}}(\lambda_{\mathrm{A}})(\lambda_{\mathrm{A}} - \lambda_{\mathrm{D,eq}}), \tag{39}$$

where $\underline{\underline{\boldsymbol{S}}}_{\mathrm{D}} = \underline{\underline{\boldsymbol{Q}}}_{\mathrm{D}} / \operatorname{tr} \underline{\underline{\boldsymbol{Q}}}_{\mathrm{D}}$ is the (unit trace) orientation tensor of the detached population, and λ_{A} is defined in Equation (27). The first term of the RHS is the flow contribution to the stretch, the second term is the stretch relaxation with a characteristic time τ_{s} and includes finite extensibility, and the last term is a source term which is proportional to the fraction of attached chains and the rate of detachment. It accounts for the additional stretch that an attached chain brings to the detached population when it detaches.

We then need to split the CCR rate up into two contributions. A first contribution comes from the detached chains similar to Equation (38), but using $\lambda_{\mathrm{D,eq}}$

$$\nu_1 = (1-f)\frac{1-\lambda_{\mathrm{D,eq}}^{-1}}{\tau_{\mathrm{s}}}\mathrm{fene}(\lambda_{\mathrm{D,eq}}). \tag{40}$$

A second contribution, ν_2, to the total CCR rate comes from the detachment of (attached) stretched chains as

$$\nu_2 = fr_{\mathrm{as}\to\mathrm{free}}(\lambda_{\mathrm{A}})\frac{\lambda_{\mathrm{A}}-\lambda_{\mathrm{D}}}{(\lambda_{\mathrm{A}}+\lambda_{\mathrm{D}})/2}. \tag{41}$$

We need to include this second contribution because, in the stochastic model, when a chain detaches, it loses stretch (sometimes rapidly) before "joining" the average of the detached population. During this detachment and retraction process, it contributes significantly to CCR, and we capture this through Equation (41).
With Equations (40) and (41), the total CCR rate of the pre-averaged model matches reasonably closely the stochastic model in all regimes of the parameter space.

E. Pre-averaged equation set

The time evolution equations of the fraction of attached chains, of the tensors $\underline{\underline{\boldsymbol{Q}}}_{\mathrm{A}}$ and $\underline{\underline{\boldsymbol{Q}}}_{\mathrm{D}}$ – as the sum of the flow terms Equations (36) and (37), and exchange terms Equations (30) and (31) – are summarized below:

Pre-averaged Equation Set

Expression for the stress tensor, in units of G:

$$\underline{\underline{\boldsymbol{\sigma}}} = f\underline{\underline{\boldsymbol{Q}}}_{\mathrm{A}} + (1-f)\underline{\underline{\boldsymbol{Q}}}_{\mathrm{D}} \quad .$$

Evolution of the fraction of attached chains:

$$\frac{\mathrm{d}f}{\mathrm{d}t} = r_{\mathrm{free}\to\mathrm{as}}\,(1-f) - r_{\mathrm{as}\to\mathrm{free}}(\lambda_{\mathrm{A}})f.$$

Evolution of the attached chains tensor:

$$\frac{\mathrm{d}\underline{\underline{\boldsymbol{Q}}}_{\mathrm{A}}}{\mathrm{d}t} = \underline{\underline{\boldsymbol{g}}}(\underline{\underline{\boldsymbol{Q}}}_{\mathrm{A}}) + \frac{1}{3\lambda_{\max}^2 - 3}\,\mathrm{tr}\left[\underline{\underline{\boldsymbol{g}}}(\underline{\underline{\boldsymbol{Q}}}_{\mathrm{A}})\right]\underline{\underline{\boldsymbol{Q}}}_{\mathrm{A}} + r_{\mathrm{free}\to\mathrm{as}}\frac{1-f}{f}\left(\underline{\underline{\boldsymbol{Q}}}_{\mathrm{D}} - \underline{\underline{\boldsymbol{Q}}}_{\mathrm{A}}\right),$$

with

$$\underline{\underline{\boldsymbol{g}}}(\underline{\underline{\boldsymbol{Q}}}_{\mathrm{A}}) \equiv \underline{\underline{\boldsymbol{\kappa}}}\cdot\underline{\underline{\boldsymbol{Q}}}_{\mathrm{A}} + \underline{\underline{\boldsymbol{Q}}}_{\mathrm{A}}\cdot\underline{\underline{\boldsymbol{\kappa}}}^{\mathrm{T}} - \beta\tilde{\nu}\lambda_{\mathrm{A}}^{-1}\left(\underline{\underline{\boldsymbol{Q}}}_{\mathrm{A}} - \mathrm{fene}(\lambda_{\mathrm{A}})\underline{\underline{\boldsymbol{I}}}\right).$$

Evolution of the detached chains tensor:

$$\frac{\mathrm{d}\underline{\underline{\boldsymbol{Q}}}_{\mathrm{D}}}{\mathrm{d}t} = \underline{\underline{\boldsymbol{h}}}(\underline{\underline{\boldsymbol{Q}}}_{\mathrm{D}}) + \frac{1}{3\lambda_{\max}^2 - 3}\,\mathrm{tr}\left[\underline{\underline{\boldsymbol{h}}}(\underline{\underline{\boldsymbol{Q}}}_{\mathrm{D}})\right]\underline{\underline{\boldsymbol{Q}}}_{\mathrm{D}} + r_{\mathrm{as}\to\mathrm{free}}(\lambda_{\mathrm{A}})\frac{f}{1-f}\left(\underline{\underline{\boldsymbol{Q}}}_{\mathrm{A}} - \underline{\underline{\boldsymbol{Q}}}_{\mathrm{D}}\right),$$

with

$$\begin{aligned}\underline{\underline{\boldsymbol{h}}}(\underline{\underline{\boldsymbol{Q}}}_{\mathrm{D}}) \equiv\ & \underline{\underline{\boldsymbol{\kappa}}}\cdot\underline{\underline{\boldsymbol{Q}}}_{\mathrm{D}} + \underline{\underline{\boldsymbol{Q}}}_{\mathrm{D}}\cdot\underline{\underline{\boldsymbol{\kappa}}}^{\mathrm{T}} - \beta\tilde{\nu}\lambda_{\mathrm{D}}^{-1}\left(\underline{\underline{\boldsymbol{Q}}}_{\mathrm{D}} - \mathrm{fene}(\lambda_{\mathrm{D}})\underline{\underline{\boldsymbol{I}}}\right)\\ & - \frac{1}{\tau_{\mathrm{d}}}\left(\underline{\underline{\boldsymbol{Q}}}_{\mathrm{D}} - \mathrm{fene}(\lambda_{\mathrm{D}})\underline{\underline{\boldsymbol{I}}}\right) - \frac{2(1-\lambda_{\mathrm{D}}^{-1})}{\tau_{\mathrm{s}}}\mathrm{fene}(\lambda_{\mathrm{D}})\underline{\underline{\boldsymbol{Q}}}_{\mathrm{D}}.\end{aligned}$$

Pre-averaged CCR rate:

$$\tilde{\nu} = 2(1-f)\frac{1-\lambda_{\mathrm{D,eq}}^{-1}}{\tau_{\mathrm{s}}}\mathrm{fene}(\lambda_{\mathrm{D,eq}}) + f r_{\mathrm{as}\to\mathrm{free}}(\lambda_{\mathrm{A}})\frac{\lambda_{\mathrm{A}} - \lambda_{\mathrm{D}}}{(\lambda_{\mathrm{A}} + \lambda_{\mathrm{D}})/2}.$$

Evolution of the CCR stretch-variable:

$$\frac{\mathrm{d}\lambda_{\mathrm{D,eq}}}{\mathrm{d}t} = (\underline{\underline{\boldsymbol{\kappa}}} : \underline{\underline{\boldsymbol{Q}}}_{\mathrm{D}} / \,\mathrm{tr}\,\underline{\underline{\boldsymbol{Q}}}_{\mathrm{D}})\lambda_{\mathrm{D,eq}} - \frac{\lambda_{\mathrm{D,eq}} - 1}{\tau_{\mathrm{s}}}\mathrm{fene}(\lambda_{\mathrm{D,eq}}) + f r_{\mathrm{as}\to\mathrm{free}}(\lambda_{\mathrm{A}})(\lambda_{\mathrm{A}} - \lambda_{\mathrm{D,eq}}).$$

Rate of detachment:

$$r_{\mathrm{as}\to\mathrm{free}}(\lambda_{\mathrm{A}}) = \tau_{\mathrm{as}}^{-1}\left(\frac{1-\lambda_{\mathrm{A}}^2\lambda_{\max}^{-2}}{1-\lambda_{\max}^{-2}\left(\lambda_{\mathrm{A}} - \frac{r}{Za_0}\right)^2}\right)^{-\frac{3}{2}Z\lambda_{\max}^2} \quad .$$

Stretch of the attached and detached chains:

$$\lambda_{\mathrm{A}} = \left(\frac{\lambda_{\max}^2\,\mathrm{tr}\left(\underline{\underline{\boldsymbol{Q}}}_{\mathrm{A}}\right)}{3\lambda_{\max}^2 - 3 + \mathrm{tr}\left(\underline{\underline{\boldsymbol{Q}}}_{\mathrm{A}}\right)}\right)^{1/2}, \qquad \lambda_{\mathrm{D}} = \left(\frac{\lambda_{\max}^2\,\mathrm{tr}\left(\underline{\underline{\boldsymbol{Q}}}_{\mathrm{D}}\right)}{3\lambda_{\max}^2 - 3 + \mathrm{tr}\left(\underline{\underline{\boldsymbol{Q}}}_{\mathrm{D}}\right)}\right)^{1/2} .$$

F. Predictions of the pre-averaged model

We solved the pre-averaged equation set of ODEs presented in the previous section using the Euler scheme, with a time step $\Delta t < \min(\tau_{\rm as}, \tau_{\rm free}, \tau_{\rm s}, \kappa^{-1})/100$, where $\kappa = \dot{\gamma}$ or $\dot{\varepsilon}$ is the flow rate.

We present in Figures 12–16 the predictions of the pre-averaged model for the regions A_1, A_2, B, C_1, and C_2 respectively.

It is evident that the pre-averaged model captures most of the features of the stochastic model:

(i) we obtain the same critical shear rate, $\dot{\gamma}_{\rm c}^{\rm hard}$, at which shear hardening is seen;

(ii) transients in regions A_1, A_2, and B are in almost perfect quantitative agreement;

(iii) steady state stress as a function of shear rate curves have the same trend;

(iv) the spikes at intermediate elongation rate in region A_1, Figure 12, are well resolved.

Although the pre-averaged model successfully captures the onset of the spikes in the regions C_1 and C_2, it suffers from the biggest discrepancies at intermediate (shear or elongation) rates with to the stochastic predictions.

In the region C_1, Figure 15, the pre-averaged model produces oscillations in shear that are not present in Figure 10 for $\dot{\gamma} = 0.3$ and $\dot{\gamma} = 0.5$.

In the region C_2, Figure 16, the undershoots, both in elongation and shear, are not captured, and the steady state stresses are different at low and intermediate flow rates.

It is, of course, extremely unlikely that a pre-averaged model could quantitatively capture every single feature of the stochastic model. We consider the remarkably high level of agreement between the stochastic and pre-averaged models to be a significant success of this work. As a result, we have a model which is suitable for flow computation, with physically meaningful parameters, that can be used as a "toy" model for future investigations.

G. Constitutive curve comparison

In Figure 17, we present the steady state shear and elongation stresses as a function of the flow rate obtained by averaging out the late time values of the stress tensor: σ_{xy} in shear, and $\sigma_{xx} - \sigma_{yy}$ in elongation, for both the stochastic and pre-averaged model. We note

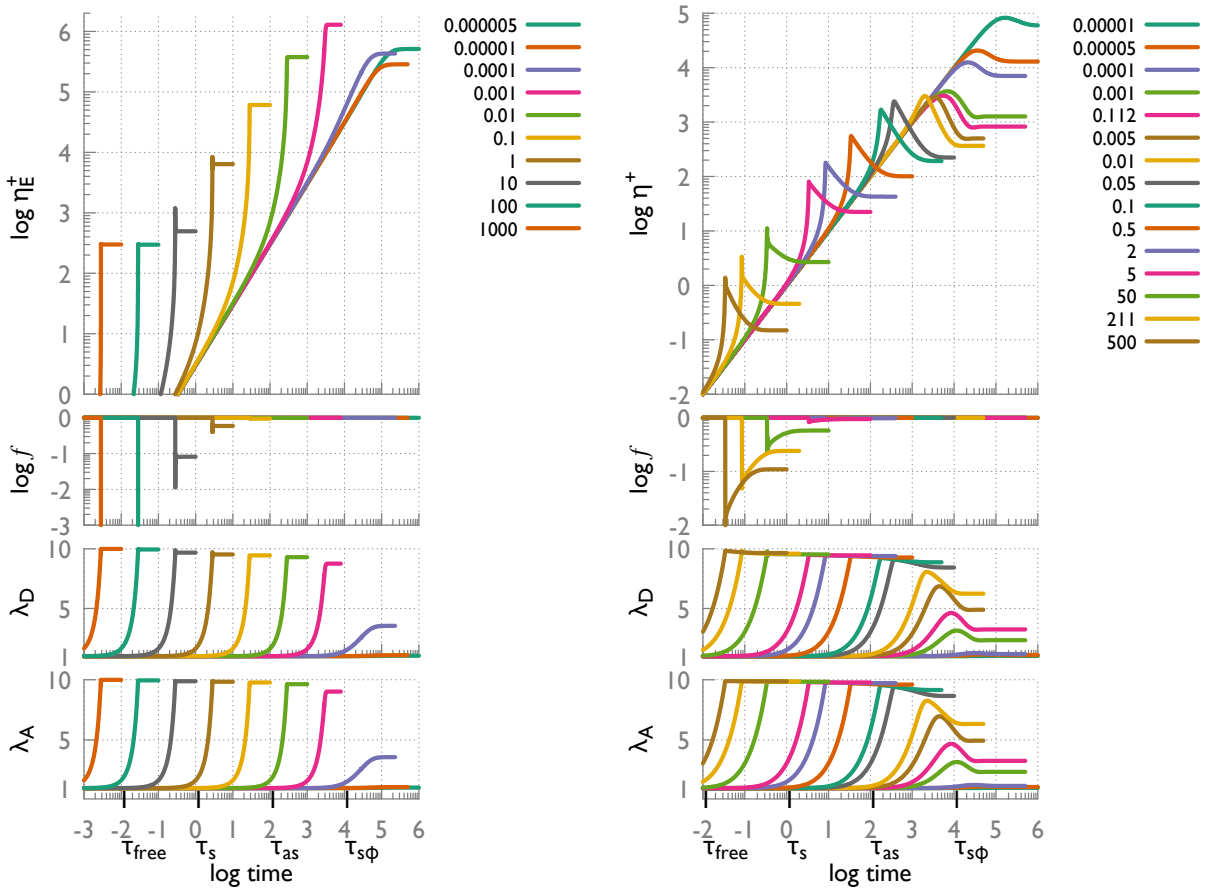

(a) Elongation (b) Shear

FIG. 12. Pre-averaged model predictions for region A_1 in the non-linear regime. We present the values, as a function of time, of the fraction of attached chains, f, the stretch of the attached chains λ_A and stretch of the detached chains λ_D, and stress growth coefficients, η_E^+ and η^+, for uniaxial extension (left), and step rate (right) respectively. Parameters are $\tau_{free} = 10^{-2}$, $\tau_{as} = 10^2$, $\tau_s = 1$, $\tau_d = 10^6$ $\lambda_{max} = 10$.

that

(i) In regions A_2 and B, there is a perfect agreement between the stochastic and pre-averaged model in both shear and elongation.

(ii) In region C_2 there is qualitative agreement of the steady state stresses between the stochastic and pre-averaged model.

(iii) In region A_1, the pre-averaged model predicts slightly negative slope in shear and elongation which are not seen in the stochastic model. This is caused by a too high CCR rate

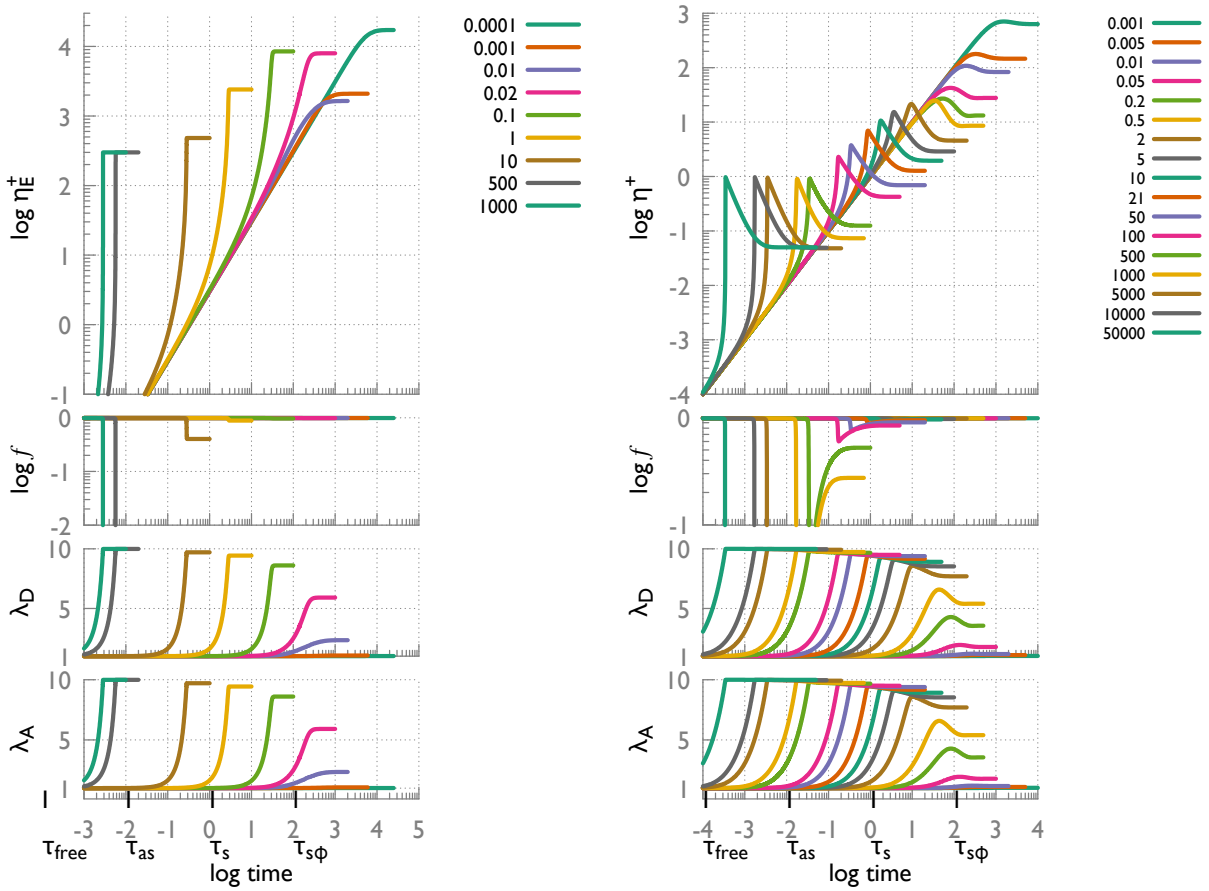

(a) Elongation

(b) Shear

FIG. 13. Pre-averaged model predictions for region A_2 in the non-linear regime. We present the values, as a function of time, of the fraction of attached chains, f, the stretch of the attached chains λ_A and stretch of the detached chains λ_D, and stress growth coefficients, η_E^+ and η^+, for uniaxial extension (left), and step rate (right) respectively. Parameters are $\tau_{free} = 10^{-4}$, $\tau_{as} = 10^{-2}$, $\tau_s = 1$, $\tau_d = 10^6$ $\lambda_{max} = 10$.

in the pre-averaged model which results in a higher stress value.

(iv) Due to the CCR parameter being large enough ($\beta = 1$), the regions A_1, A_2, and B exhibit a monotonic curve. However, the region C_2 shows a clearly non-monotonic relation between steady state stress and shear rate, in both the stochastic and pre-averaged model, which, according to recent works, implies shear banding of the system in the steady state [43–46]. Also, transient shear banding might occur where shear hardening and rapid stress drop is seen.

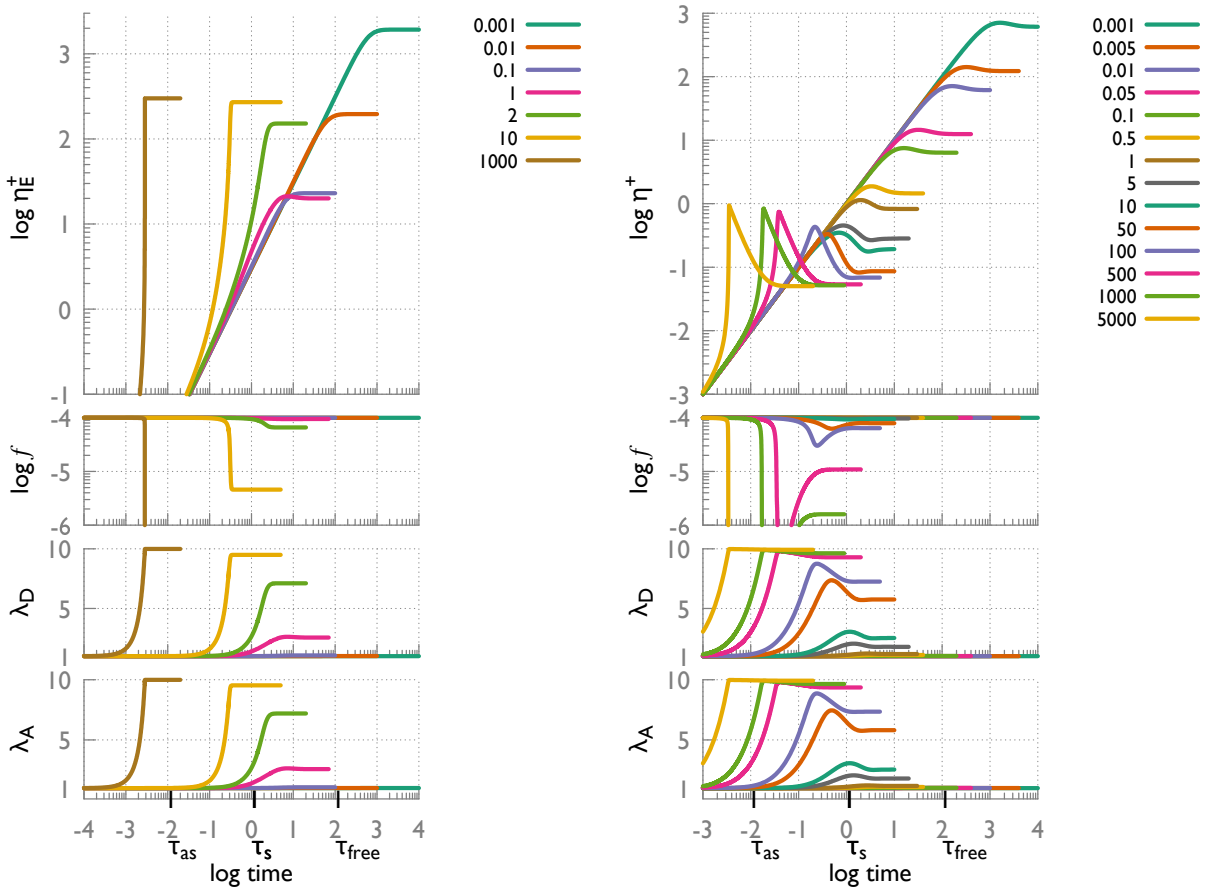

(a) Elongation

(b) Shear

FIG. 14. Pre-averaged model predictions for region B in the non-linear regime. We present the values, as a function of time, of the fraction of attached chains, f, the stretch of the attached chains λ_A and stretch of the detached chains λ_D, and stress growth coefficients, η_E^+ and η^+, for uniaxial extension (left), and step rate (right) respectively. Parameters are $\tau_{free} = 10^2$, $\tau_{as} = 10^{-2}$, $\tau_s = 1$, $\tau_d = 10^6$ $\lambda_{max} = 10$.

(v) Results presented in this work for the region C_1 are for $\phi = 0.01$, and do not present a non-monotonic relation for the stochastic model. However, we already see an onset of non-monotonicity in the pre-averaged model. As we go towards region C_2 (e.g. increasing ϕ), the non-monotonicity starts to grow. Therefore, we might be able to tune the shear banding properties of the polymeric systems by adjusting the parameter ϕ.

In a further work, we shall address these questions of stability and shear banding of the

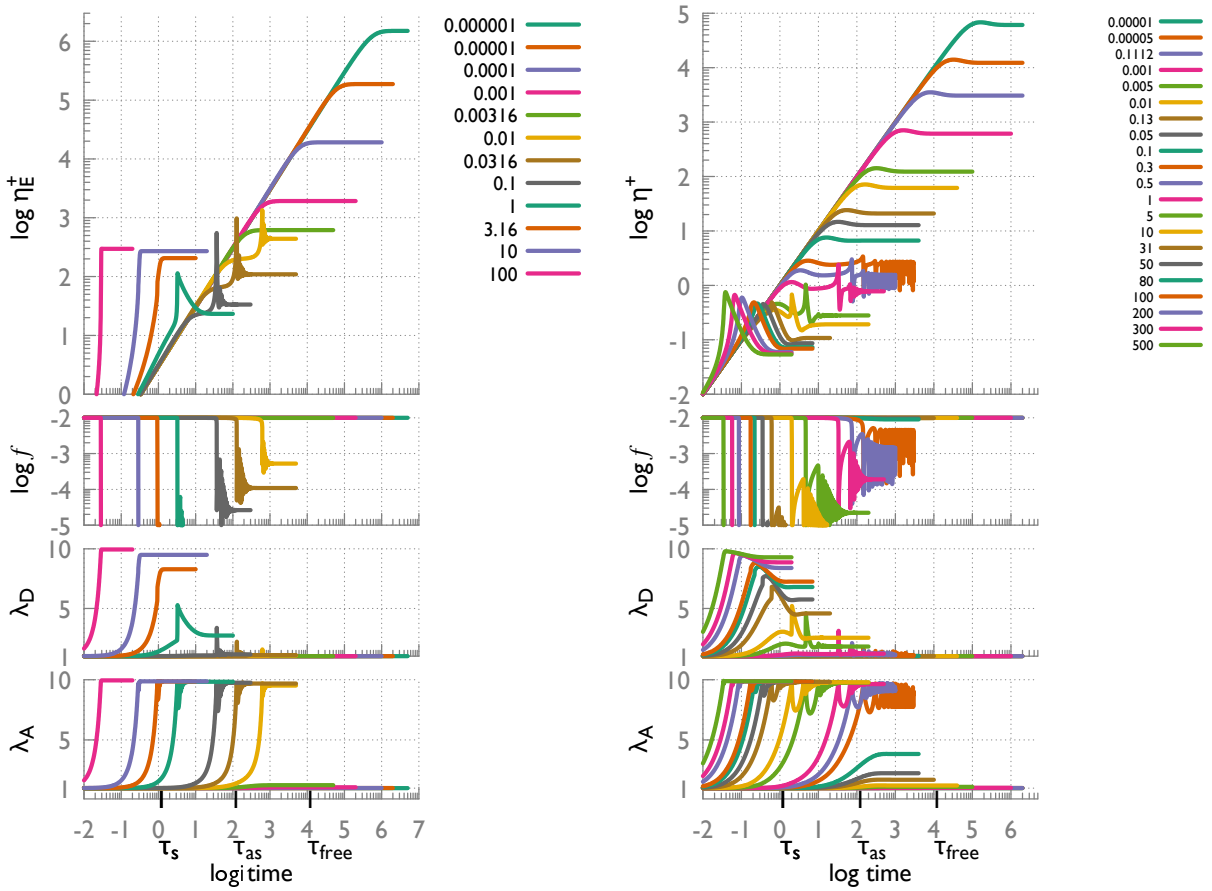

(a) Elongation

(b) Shear

FIG. 15. Pre-averaged model predictions for region C_1 in the non-linear regime. We present the values, as a function of time, of the fraction of attached chains, f, the stretch of the attached chains λ_A and stretch of the detached chains λ_D, and stress growth coefficients, η_E^+ and η^+, for uniaxial extension (left), and step rate (right) respectively. Parameters are $\tau_{free} = 10^4$, $\tau_{as} = 10^2$, $\tau_s = 1$, $\tau_d = 10^6$ $\lambda_{max} = 10$.

system in the different quadrants of Figure 6.

VI. CONCLUSIONS

The central goal of this work was to produce a simplified non-linear constitutive "toy" model which could capture effects of both entanglements and "sticky" telechelic groups in polymeric systems. As argued in the introduction, we chose the star polymer as the simplest architecture to consider, since it results in a two-state system in which the single sticker is

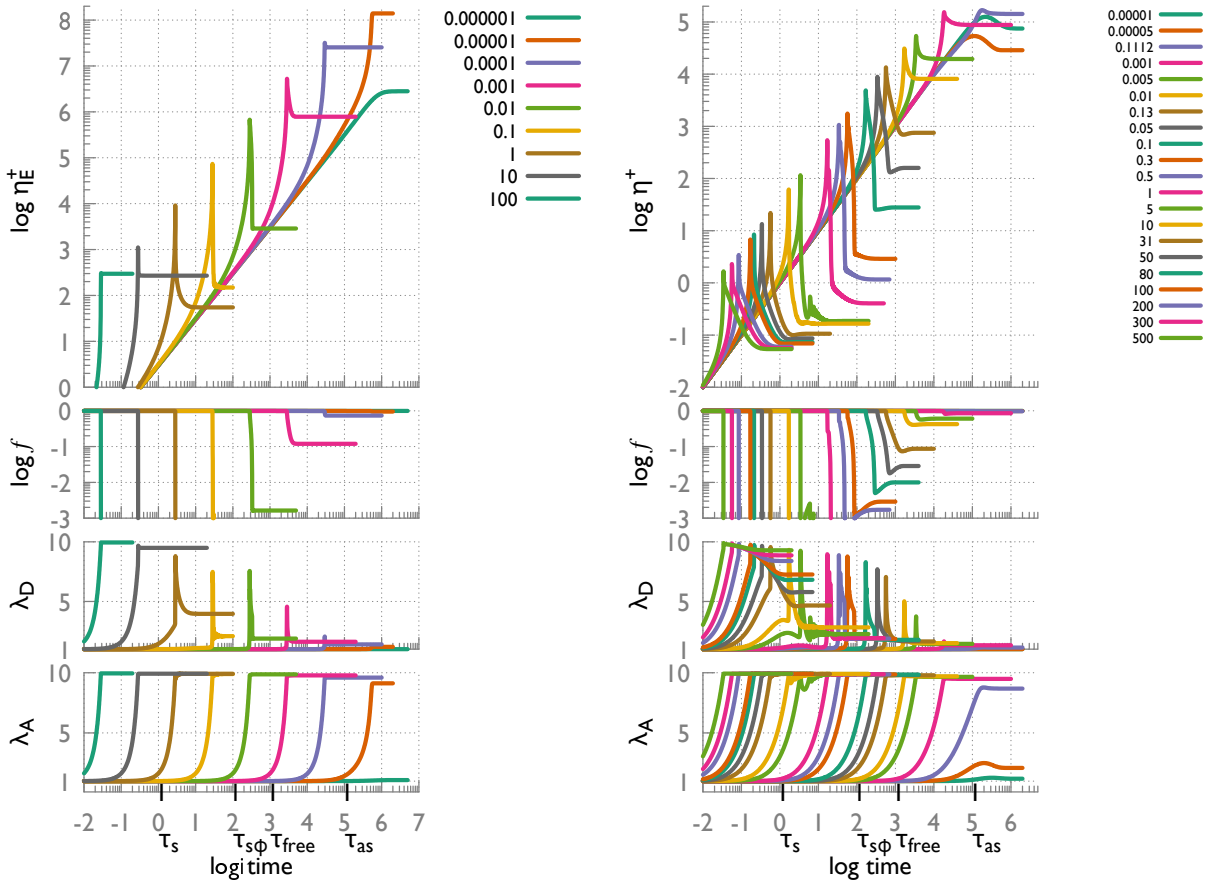

(a) Elongation

(b) Shear

FIG. 16. Pre-averaged model predictions for region C_2 in the non-linear regime. We present the values, as a function of time, of the fraction of attached chains, f, the stretch of the attached chains λ_A and stretch of the detached chains λ_D, and stress growth coefficients, η_E^+ and η^+, for uniaxial extension (left), and step rate (right) respectively. Parameters are $\tau_{free} = 10^3$, $\tau_{as} = 10^5$, $\tau_s = 1$, $\tau_d = 10^6$ $\lambda_{max} = 10$.

attached or detached. Our methodology, then, was to create a stochastic model in which each star arm has its own history of attachment and detachment, and then to create a pre-averaged model with properties that closely resemble the stochastic system. Both models contain physically meaningful parameters, allowing a "map" of typical behavior in different regions of parameter space to be investigated.

The simplified stochastic tube model for entangled telechelic stars exhibits a broad range of behaviors that one is able to tune by adjusting the sticker parameters, τ_{as}, and τ_{free}

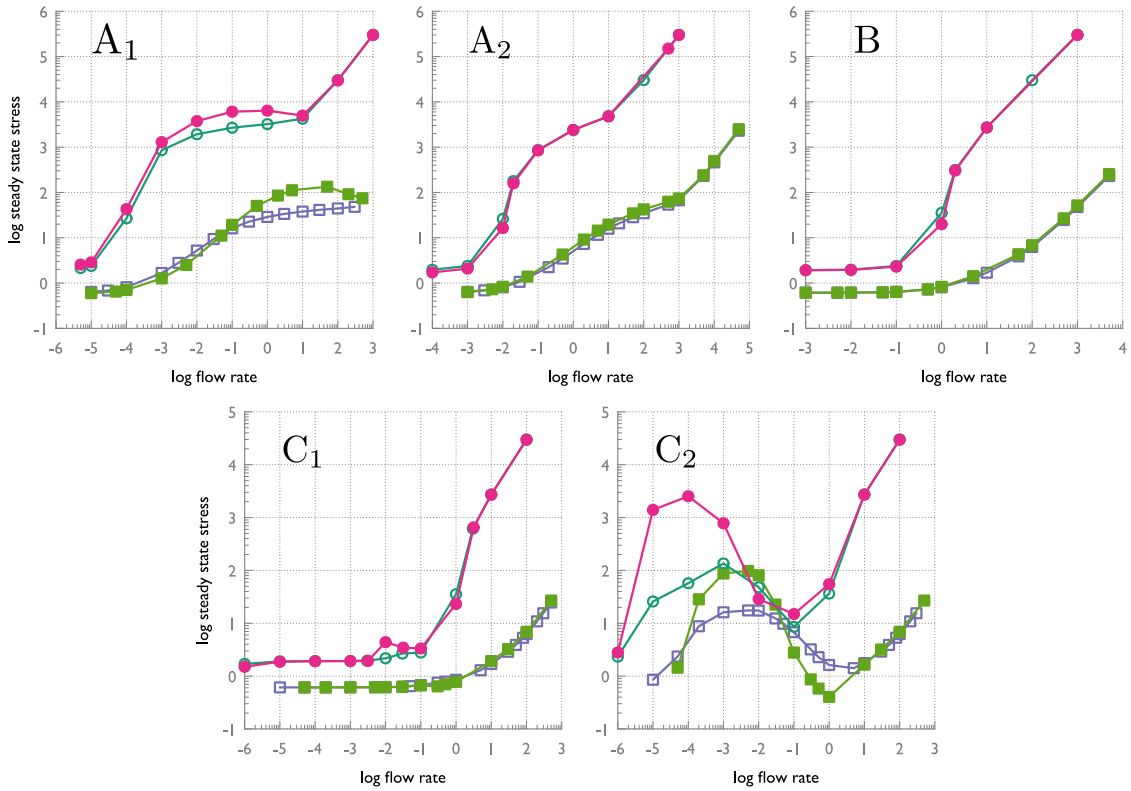

FIG. 17. Steady state stress as a function of the flow rate in the different regions of Figure 6, in shear (σ_{xy}) and elongation ($\sigma_{xx} - \sigma_{yy}$), squares and circles respectively. Comparison between the stochastic model (empty symbols) and pre-averaged model (filled symbols).

with respect to the orientation (in the linear regime) or stretch (in the non-linear regime) relaxation times. In both the linear and non-linear regime, we produced a parameter map where we identified different regions defined by how critical timescales compare. In the linear regime, our model is in good agreement with the more detailed work of van Ruymbeke and co-workers [2].

In the non-linear regime, we saw dramatic changes in the stress growth coefficient transients as we navigated around the parameter map, i.e. our constitutive model exhibits a rich variety of responses. We observed that particular parameter sets produce shear hardening, extension hardening, sharp stress drops, smoother stress drops, monotonic and non-monotonic curve for the steady state stress as a function of shear rate.

Finally, we developed a pre-averaged model, that retains the vast majority of the features of the stochastic model. We anticipate that this will serve as a prototypical "toy" model for flow computation. As an example of this, our immediate future intention is to investigate

flow instabilities such as shear banding using this novel constitutive model.

ACKNOWLEDGEMENT

The work leading to these results has received funding from the People Programme (Marie Skłodowska-Curie Actions) of the European Union's Seventh Framework Programme (FP7/2007-2013) under REA grant agreement n° 607937 – SUPOLEN project.

---

[1] Likhtman, A. E., and R. S. Graham, "Simple constitutive equation for linear polymer melts derived from molecular theory: Rolie-Poly equation," *J. Nonnewton. Fluid Mech.* **114**, 1–12 (2003).

[2] van Ruymbeke, E., D. Vlassopoulos, M. Mierzwa, T. Pakula, D. Charalabidis, M. Pitsikalis, and N. Hadjichristidis, "Rheology and structure of entangled telechelic linear and star polyisoprene melts," *Macromolecules* **43**, 4401–4411 (2010).

[3] Uraneck, C. A., H. L. Hsieh, and O. G. Buck, "Telechelic polymers," *J. Polym. Sci.* **46**, 535–539 (1960).

[4] Semenov, A. N., J.-F. Joanny, and A. R. Khokhlov, "Associating polymers: equilibrium and linear viscoelasticity," *Macromolecules* **28**, 1–10 (1995).

[5] Tripathi, A., K. C. Tam, and G. H. McKinley, "Rheology and Dynamics of Associate Polymer Solutions in Shear and Extension: Theory and Experiments," *Macromolecules* **39**, 1981–1999 (2006).

[6] Semenov, A. N., and M. Rubinstein, "Thermoreversible Gelation in Solutions of Associative Polymers. 1. Statics," *Macromolecules* **31**, 1373–1385 (1998).

[7] Rubinstein, M., and A. N. Semenov, "Thermoreversible Gelation in Solutions of Associating Polymers. 2. Linear Dynamics," *Macromolecules* **31**, 1386–1397 (1998).

[8] Semenov, A. N., I. A. Nyrkova, and A. R. Khokhlov, "Polymers with Strongly Interacting Groups: Theory for Nonspherical Multiplets," *Macromolecules* **28**, 7491–7500 (1995).

[9] Leibler, L., M. Rubinstein, and R. H. Colby, "Dynamics of Reversible Networks," *Macromolecules* **24**, 4701–4707 (1991).

[10] Rubinstein, M., and A. N. Semenov, "Dynamics of Entangled Solutions of Associating Polymers," *Macromolecules* **34**, 1058–1068 (2001).

[11] Baxandall, L. G., "Dynamics of reversibly crosslinked chains," *Macromolecules* **22**, 1982–1988 (1989).

[12] Bick, D. K., and T. C. B. McLeish, "Topological Contributions to Nonlinear Elasticity in Branched Polymers," *Phys. Rev. Lett.* **76**, 2587–2590 (1996).

[13] McLeish, T. C. B., and R. G. Larson, "Molecular constitutive equations for a class of branched polymers: The pom-pom polymer," *J. Rheol.* **42**, 81–110 (1998).

[14] Wagner, M. H., and V. H. Rolon-Garrido, "Verification of branch point withdrawal in elongational flow of pom-pom polystyrene melt," *J. Rheol.* **52**, 1049–1068 (2008).

[15] Hawke, L. G. D., Q. Huang, O. Hassager, and D. J. Read, "Modifying the pom-pom model for extensional viscosity overshoots," *J. Rheol.* **59**, 995–1017 (2015).

[16] Marrucci, G., "Dynamics of entanglements: A nonlinear model consistent with the Cox-Merz rule," *J. Nonnewton. Fluid Mech.* **62**, 279–289 (1996).

[17] Cates, M. E., "Nonlinear viscoelasticity of wormlike micelles (and other reversibly breakable polymers)," *J. Phys. Chem.* **94**, 371–375 (1990).

[18] Tam, K. C., R. D. Jenkins, M. A. Winnik, and D. R. Bassett, "A Structural Model of Hydrophobically Modified Urethane-Ethoxylate (HEUR) Associative Polymers in Shear Flows," *Macromolecules* **31**, 4149–4159 (1998).

[19] Fetters, L. J., W. W. Graessley, N. Hadjichristidis, A. D. Kiss, D. S. Pearson, and L. B. Younghouse, "Association behavior of end-functionalized polymers. 2. Melt rheology of polyisoprenes with carboxylate, amine, and zwitterion end groups," *Macromolecules* **21**, 1644–1653 (1988).

[20] Vlassopoulos, D., T. Pakula, G. Fytas, M. Pitsikalis, and N. Hadjichristidis, "Controlling the self-assembly and dynamic response of star polymers by selective telechelic functionalization," *J. Chem. Phys.* **111**, 1760–1764 (1999).

[21] Vlassopoulos, D., M. Pitsikalis, and N. Hadjichristidis, "Linear Dynamics of End-Functionalized Polymer Melts: Linear Chains, Stars, and Blends," *Macromolecules* **33**, 9740–9746 (2000).

[22] Milner, S. T., and T. C. B. McLeish, "Parameter-Free Theory for Stress Relaxation in Star Polymer Melts," *Macromolecules* **30**, 2159–2166 (1997).

[23] Ball, R. C., and T. C. B. McLeish, "Dynamic dilution and the viscosity of star-polymer melts," *Macromolecules* **22**, 1911–1913 (1989).

[24] McLeish, T. C. B., and S. T. Milner, "Entangled Dynamics and Melt Flow of Branched Polymers," *Branched Polym. II*, (Springer Berlin Heidelberg, Berlin, Heidelberg, 1999), 195–256.

[25] Schaefgen, J. R., and P. J. Flory, "Synthesis of Multichain Polymers and Investigation of their Viscosities," *J. Am. Chem. Soc.* **70**, 2709–2718 (1948).

[26] Morton, M., T. E. Helminiak, S. D. Gadkary, and F. Bueche, "Preparation and properties of monodisperse branched polystyrene," *J. Polym. Sci.* **57**, 471–482 (1962).

[27] Hadjichristidis, N., M. Pitsikalis, H. Iatrou, P. Driva, G. Sakellariou, and M. Chatzichristidi, "Polymers with Star-Related Structures," *Polym. Sci. A Compr. Ref.*, (Elsevier, Amsterdam, 2012), 29–111.

[28] Ren, J. M., T. G. McKenzie, Q. Fu, E. H. H. Wong, J. Xu, Z. An, S. Shanmugam, T. P. Davis, C. Boyer, and G. G. Qiao, "Star Polymers," *Chem. Rev.* **116**, 6743–6836 (2016).

[29] Green, M. S., and A. V. Tobolsky, "A New Approach to the Theory of Relaxing Polymeric Media," *J. Chem. Phys.* **14**, 80–92 (1946).

[30] Graham, R. S., A. E. Likhtman, T. C. B. McLeish, and S. T. Milner, "Microscopic theory of linear, entangled polymer chains under rapid deformation including chain stretch and convective constraint release," *J. Rheol.* **47**, 1171–1200 (2003).

[31] Mead, D. W., R. G. Larson, and M. Doi, "A Molecular Theory for Fast Flows of Entangled Polymers," *Macromolecules* **31**, 7895–7914 (1998).

[32] Ianniruberto, G., and G. Marrucci, "A multi-mode CCR model for entangled polymers with chain stretch," *J. Nonnewton. Fluid Mech.* **102**, 383–395 (2002).

[33] Warner, H. R., "Kinetic Theory and Rheology of Dilute Suspensions of Finitely Extendible Dumbbells," *Ind. Eng. Chem. Fundam.* **11**, 379–387 (1972).

[34] Rubinstein, M., and S. Panyukov, "Nonaffine Deformation and Elasticity of Polymer Networks," *Macromolecules* **30**, 8036–8044 (1997).

[35] Everaers, R., "Topological versus rheological entanglement length in primitive-path analysis protocols, tube models, and slip-link models," *Phys. Rev. E* **86**, 022801 (2012).

[36] Heinrich, G., and M. Kaliske, "Theoretical and numerical formulation of a molecular based constitutive tube-model of rubber elasticity," *Comput. Theor. Polym. Sci.* **7**, 227–241 (1997).

[37] Brassinne, J., C.-A. Fustin, and J.-F. Gohy, "Polymer Gels Constructed Through Metal-Ligand Coordination," *J. Inorg. Organomet. Polym. Mater.* **23**, 24–40 (2013).

[38] Hernández Cifre, J. G., T. M. A. O. M. Barenbrug, J. D. Schieber, and B. H. A. A. van den Brule, "Brownian dynamics simulation of reversible polymer networks under shear using a non-interacting dumbbell model," *J. Nonnewton. Fluid Mech.* **113**, 73–96 (2003).

[39] Doi, M., and S. F. Edwards, *The Theory of Polymer Dynamics*, (Oxford University Press Inc., New York, 1988).

[40] Schwarzl, F. R., "Numerical calculation of storage and loss modulus from stress relaxation data for linear viscoelastic materials," *Rheol. Acta* **10**, 165–173 (1971).

[41] Snijkers, F., K. Ratkanthwar, D. Vlassopoulos, and N. Hadjichristidis, "Viscoelasticity, nonlinear shear start-up, and relaxation of entangled star polymers," *Macromolecules* **46**, 5702–5713 (2013).

[42] Vaccaro, A., and G. Marrucci, "A model for the nonlinear rheology of associating polymers," *J. Nonnewton. Fluid Mech.* **92**, 261–273 (2000).

[43] Adams, J. M., S. M. Fielding, and P. D. Olmsted, "Transient shear banding in entangled polymers: A study using the Rolie-Poly model," *J. Rheol.* **55**, 1007–1032 (2011).

[44] Moorcroft, R. L., and S. M. Fielding, "Criteria for Shear Banding in Time-Dependent Flows of Complex Fluids," *Phys. Rev. Lett.* **110**, 086001 (2013).

[45] Cromer, M., G. H. Fredrickson, and L. G. Leal, "A study of shear banding in polymer solutions," *Phys. Fluids* **26**, 063101 (2014).

[46] Fielding, S. M., "Triggers and signatures of shear banding in steady and time-dependent flows," *J. Rheol.* **60**, 821–834 (2016).